NUMERICAL AND EXPERIMENTAL INVESTIGATION OF WAVY LEADING EDGE MODIFICATIONS ON NACA0012 AIRFOIL PERFORMANCE

KAAN GUZEY

SEPTEMBER 2022

CANKAYA UNIVERSITY

GRADUATE SCHOOL OF NATURAL AND APPLIED SCIENCES

DEPARTMENT OF MECHANICAL ENGINEERING
MASTER'S THESIS IN
MECHANICAL ENGINEERING

NUMERICAL AND EXPERIMENTAL INVESTIGATION OF WAVY
LEADING EDGE MODIFICATIONS ON NACA0012 AIRFOIL
PERFORMANCE

KAAN GUZEY

SEPTEMBER 2022

ABSTRACT

NUMERICAL AND EXPERIMENTAL INVESTIGATION OF WAVY LEADING EDGE MODIFICATIONS ON NACA0012 AIRFOIL PERFORMANCE

GÜZEY, Kaan

M.Sc., Department of Mechanical Engineering

Supervisor: Assoc. Prof.Dr. Ece Aylı

Co-Supervisor: Prof.Dr. Selin Aradağ Çelebioğlu

September 2022, 79 Page

This thesis presents numerical and experimental studies on aerodynamic and aeroacoustic characteristics of the NACA0012 profile. The leading-edge serrations under investigation are in a sinusoidal profile with two main design parameters of wavelength and amplitude. Noise suppressing ability of sinusoidal serrations is the function of several parameters like amplitude, wavelength, inflow speed, angle of attack and frequency range which are examined in this thesis. Amplitude and wavelength of the serration are varied between $1.25 < A < 2.5$, $20 < \lambda < 60$, respectively. The corresponding Reynolds numbers are between 1×10^5 and 3×10^5, respectively. The angle of attack for each configuration is changed between $4° < aoa < 16°$. 40 configurations are tested in this study. According to the results, owl-inspired leading-edge serrations can be used as aero-acoustic control add-ons in blade designs for wind turbines, aircraft, and fluid machinery. Results depicted that the narrower and sharper serrations have a better noise reduction effect. In the configuration with the largest amplitude and smaller wavelength, overall SPL reduces up to 20%. Also, results showed that serration amplitude had a distinct effect on aeroacoustic performance, whereas wavelength is the function of amplitude. At the smaller angle of attack values, $aoa < 8°$, the lift and drag coefficient values are almost the same for both clean and

wavy profiles. On the other hand, typically for aoa>12°, also means that after stall increases the angle of attack, serration adversely affects aerodynamic performance.

Keywords: Airfoil, NACA0012, CFD, Experiment, LES, Serration, Wavy leading edge

ÖZ

NACA0012 PROFİLİ İÇİN DALGALI ÖN KENAR MODİFİKASYONLARININ SAYISAL VE DENEYSEL OLARAK İNCELENMESİ

GÜZEY,Kaan

Makine Mühendıslığı Yüksek Lısans

Danışman: Doç. Dr. Ece AYLI
Ortak Danışman: Prof. Dr. Selin Aradağ Çelebioğlu
Eylül 2022, 79 Sayfa

Bu tez, NACA0012 profilinin aerodinamik ve aeroakustik özellikleri üzerine sayısal ve deneysel çalışmalar sunmaktadır. İncelenmekte olan giriş kenarı tırtıkları, dalga boyu ve genlik olmak üzere iki ana tasarım parametresi ile sinüzoidal bir profildedir. Sinüzoidal dalgaların gürültü bastırma yeteneği, bu tezde incelenen genlik, dalga boyu, içeri akış hızı, hücum açısı ve frekans aralığı gibi birçok parametrenin fonksiyonudur. Tırtıkların genliği ve dalga boyu sırasıyla $1.25 < A < 2.5$, $20 < \lambda < 60$ arasında değişmektedir. Karşılık gelen Reynolds sayıları sırasıyla 1×10^5 ve 3×10^5 arasındadır. Her konfigürasyon için hücum açısı $4° <$ Hücum Açısı $< 16°$ arasında değiştirilir. Bu çalışmada 40 konfigürasyon test edilmiştir. Sonuçlara göre, baykuştan ilham alan son teknoloji tırtıklar, rüzgar türbinleri, uçak ve akışkan makineleri için kanat tasarımlarında aero-akustik kontrol eklentileri olarak kullanılabilir. Sonuçlar, daha dar ve keskin tırtıkların daha iyi bir gürültü azaltma etkisine sahip olduğunu gösterdi. En büyük genliğe ve daha küçük dalga boyuna sahip konfigürasyonda, genel SPL %20'ye kadar azaldığı gözlemlendi. Ayrıca sonuçlar, tırtıklı genliğin aeroakustik performans üzerinde belirgin bir etkisi olduğunu, dalga boyunun ise genliğin fonksiyonu olduğunu göstermiştir. Daha küçük hücum açısı değerlerinde, aoa$<8°$, hem

temiz hem de dalgalı profiller için kaldırma ve sürükleme katsayısı değerleri hemen hemen aynıdır. Öte yandan, tipik olarak aoa>12° için, aynı zamanda, stall'ın hücum açısını arttırdıktan sonra, tırtıklılığın aerodinamik performansı olumsuz etkilediği anlamına gelir.

Anahtar Kelimeler: Kanat Profili, NACA0012, HAD, Deneysel, LES, Tırtık, Tırtıklı Giriş Kanadı

ACKNOWLEDGEMENT

TABLE OF CONTENT

LIST OF TABLES

LIST OF FIGURES

LIST OF ABBREVIATIONS

CFD:	Computatioinal Fluid Dynamics
RANS:	Reynolds Averaged Navier – Stokes
URANS:	Unsteady Reynolds-Averaged Navier-Stokes
SPL:	Sound Pressure Level
LES:	Large Eddy Simulations
RMS:	Root Mean Square
FW-H:	Ffowcs Williams Hawkings
DNS:	Direct Numerical Simulations
CNC:	Computer Numerical Control
TKE:	Turbulent Kinetic Energy
FFT:	Fast Fourier Transform
AoA:	Angle of Attack
SGS:	Subgrid-scale model
PSD:	Power Spectral Density
C_L	Lift Coefficient
C_D	Drag Coefficient
T_s	Time Step
T_t	Total Analysis Time
P	Pressure
P_{Static}	Static Pressure
c	Speed of Sound in air
γ	Heat Capacity Ratio
Ma	Mach Number
SPL	Sound Pressure Level
μ_t	Eddy Viscosity
τ_{ij}	Strain Tensor
σ_{ij}	Stress Tensor
L_S	Mix Length

λ	Wavelength
W	Amplitude
c	Chord Length
St	Strouhal Number

1.   INTRODUCTION

Noise is sound waves that we encounter in our daily life and perceive as disturbing. Sound waves, on the other hand, can be defined as energy-carrying oscillations that occur in the pressure of the environment for any reason. Depending on the situation, these oscillations may be at certain frequencies, i.e. frequencies, or they may be completely random. Music contains periodic sound waves, created in an organized way, with harmony in it. Natural events such as waterfalls and sea waves create sound waves with very different frequencies that do not have harmony in most of their content, but these sounds are not disturbing because they are identified with nature by most of us. Conversely, organized (music) sound waves can cause discomfort depending on their intensity or the situation we are in. Therefore, it would be correct to say that there is a psychological dimension in the definition of noise.

In addition to negative psychological effects, it is reported that negative physiological effects such as hearing loss and blood pressure occur in people who are constantly exposed to noise. Since they create oscillations in the pressure of the environment, sound waves can also create negative effects on structures, called fatigue, according to their amplitude and frequency. Examples of this are the parts of the ship or aircraft fuselage close to the engine.

Figure 1: Turbo Blades, Wind Turbine, Turbofan

Noise has become a serious environmental problem in the world. While heavy land traffic in cities creates significant noise pollution, air traffic has intensified as air transportation has become indispensable for people and has become the most

important source of noise pollution for some cities but the effects of noise are not just ecological. Especially in the defense industry, the field of acoustics has an important place in recognizability-identification issues. Submarines, warplanes and ships and similar vehicles have become the most desirable requirements today to have low noise emissions.

Increasing noise pollution day by day has led to the need to work on noise estimation, and has been instrumental in the development of research areas such as noise due to structural vibration and aeroacoustics. Thus, noise estimation has become one of the most important research topics in the field of noise in the recent past.

Table 1.1: Effects of Sound Level on Health

CLASSIFICATION	NOISE LEVEL	OCCUPATIONAL HEALTH PROBLEM
First Degree	30-60 dB(A)	Confusion, anger, sleep and concentration disorder
Second Degree	65-90 dB(A)	Physiological responses; Increased blood pressure, heart rate and acceleration of respiration, decreased pressure in brain fluid
Third Degree	90-120 dB(A)	Increased physiological responses, headaches
Fourth Degree	120-140 dB(A)	Permanent damage to internal ear and balance deterioration
Fifth Degree	> 140 dB(A)	Serious brain destruction

The estimation of flow noise falls within the research field of aeroacoustics. Although it is directly related to fluid dynamics, the non-linearity of the equations makes noise estimation very difficult. Flow noise occurs especially with high velocity and high Reynolds number flows, where the ratio of the nonlinear terms of the equations of motion to the viscous terms is very high. It is very difficult to estimate the noise directly, since the occurrence of sound expresses the change of energy in the flow in a very short time interval. The effect of this is most observed in empty spaces and low velocity flows. However, approximate estimations can be made since the sound is produced by small fluctuations in the flow field.

The first-order approach, in which nonlinear effects are neglected, forms the basis of the acoustic concept. Thus, the concept of acoustics can be studied as a boundary value problem. In this study, the noise caused by the interaction of

turbulence in the flow with the airfoil was investigated. Turbulence is an irregular motion dominated by nonlinear convection forces. It is not possible to predict the characteristics of turbulent flows with certainty. However, in Lighthill [1] theorem, the predictability of turbulent noise can be achieved by using integral methods instead of solving differential equations. The FW-H method for estimating far-field noise is also based on the Lighthill analogy [2]. The principle of this method is to calculate the pressure changes in the far field by integrating the solution after obtaining the nonlinear pressure fluctuations on the surface of the sound source by solving the flow equations. In this study, the noise issue is handled as a part of fluid dynamics, research on computational aeroacoustics, estimation and reduction of flow noise around airfoils are included.

Aeroacoustics has started to arouse great interest in the aviation and maritime sector, which needs the estimation of flow-induced noise in recent years, with the increase in technological possibilities and processing power. The estimation of noise that will be created by aircraft wings, hydrofoils, propellers and any system that provides force in the fluid is a research subject that is needed both in environmental and military dimensions.

Figure 2: Serration geometry created by the owl and whale wings

In this study; it is aimed to estimate the turbulence-induced noise around the airfoil and to examine the effects of sinusoidal wave-shaped notch structures to be added to the edge of the tracks of the airfoil on the flow-induced noise and reduce the noise in this way. While the studies are intended to be the starting point for the noise calculations of the airfoil-based propeller, hydrofoil, aerofoil and similar geometries, it is also aimed to form the basis and knowledge in the field of computational aeroacoustics in the future.

1.1 LITERATURE SURVEY

Calculation and estimation of flow-induced noise has been the target of acoustic researchers for many years. Although the mathematical modeling of fluid dynamics and the development of solution methods date back to four hundred years ago, the first studies on flow-induced noise started with Strouhal [3] examining the noise generated by the wind around the cylinder. The first comprehensive study on computational aeroacoustics was published by Lighthill [4]. Proudman [5] also published a study on turbulence-induced noise generation in the same year. Using the analogy developed by Lighthill, Curle [6] worked on noise modeling consisting of fluid body interaction and developed the first noise model. Although these studies are insufficient for far-field noise estimation, the noise model developed by Ffowcs William and Hawkings [7] and based on the Lighthill Analogy has enabled the estimation of far-field noise. The document containing flow-induced noise measurements around airfoils, carried out by Brooks et al. [8] within NASA, has formed the basis of many computational acoustic studies, including this thesis. The document contains acoustic test results of wing profiles of different court lengths at different speeds, open and closed wing tips, and developed noise estimation methods.

Flow-induced noise in airfoils is formed by the interaction between the surface of the profile and the turbulence in the boundary layer and the traces in the edge trace region. Flow noise can be characteristically tonal or broadband. Different mechanisms can cause the formation of this noise. These mechanisms can be defined in five different ways as seen in Figure 3: Airfoil Profile Noise Generation Mechanisms
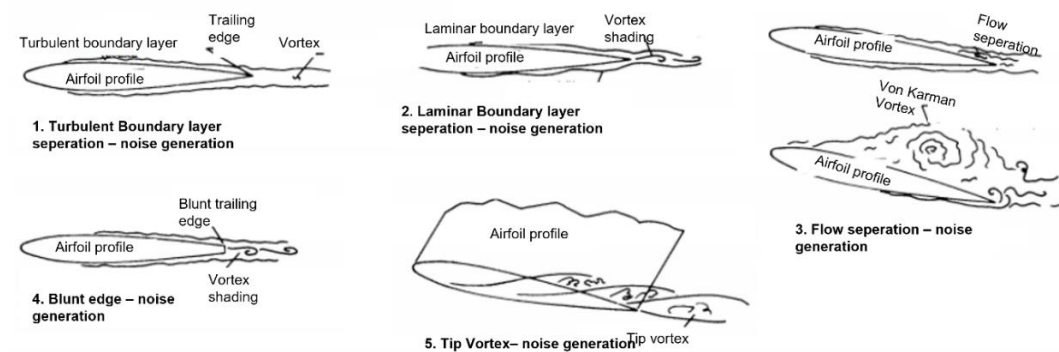
Figure 3: Airfoil Profile Noise Generation Mechanisms [9]

Since the cases generated in this study were at low angles of attack and high Reynolds numbers, it was not possible to examine the current separation noise and

4

laminar boundary layer eddy formation noises. In order to save processing power and time, since the effect of the leading edge on the flow has not been investigated, the source mechanism of the noise in the examined cases can be defined as turbulent boundary layer-traces edge noise. As can be seen in Figure 4: Effect of Leading edge vortices on noise level
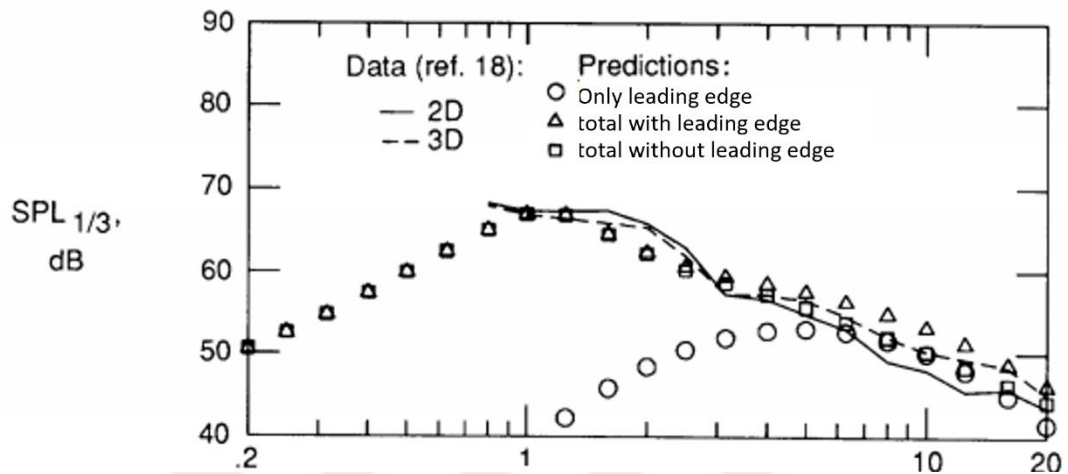
Figure 4: Effect of Leading edge vortices on noise level [10]

Many conceptual methods have emerged for the estimation of the noise generated by the mentioned noise mechanisms [11]. Two of these methods stand out. The first method is DNS (Direct Numerical Simulation) and LES (Large Eddy Simulation) solutions, which solve acoustic problems without the need for any modelling. Among them, DNS can be considered as the most definitive solution. In the DNS method, the Navier–Stokes equations are solved without the need for any modelling. However, this solution also has disadvantages. Since the processing power requirement of the DNS method increases with the third power of the Reynolds number, it is not suitable for daily use. Another disadvantage is the need for multiple scaling, which is the biggest problem in the computational aeroacoustic field. The reason for this scaling problem is that the acoustic fluctuations have very small amplitudes compared to the aerodynamic quantities and the sound velocity propagation at low Mach numbers is too high compared to the fluid velocity propagation. The second prominent method is the aforementioned hybrid methods. In this method, the formation and propagation of sound are examined separately. Sound sources, ie the formation of sound, are calculated by classical CFD methods. Apart from the LES and DES methods, which can analyze turbulence at certain rates, the

URANS method, which models turbulence, can also be used in the solution of sound formation. The methods used for the propagation of sound can calculate the noise level at certain points by integrating the acoustic pressure distributions from the CFD analysis into the far area. The first of these methods is the Lighthill Analogy. It is the most general formula used in acoustic calculations and is derived directly from the Navier-Stokes equations. According to this method, the sound source should not be located at the limits of the flow volume [12]. Since the aim is to calculate the edge noise of the tracks, this method was not considered suitable for the current study. The second method is the Curle Formulation [13]. which is created by the generalization of the Lighthill Analogy. It takes into account sources at the surface of the body as well as sources inside the flow volume. Another method in acoustic analysis is the Ffowcs Williams and Hawkings [14] formulation. Since this method takes into account the movement of the weld, it is also suitable for use with rotating bodies. Since FW-H method is the most general and reliable among the mentioned methods, this method was used in acoustic analysis within the scope of the thesis.

One of the first studies to reduce flow noise was carried out by Hersh [15] and Arndt and Nagel [16] with notch geometries added to the leading edge of the airfoil. These notches form small eddies along the profile, disrupting the periodicity of the eddy system formed at low angles of attack, thus reducing the noise [17]. However, this geometry added to the leading edge negatively affects the lift created by the airfoil and reduces the efficiency [18]. Later, Howe [19] investigated the effects of sawtooth shaped geometries added to the edge of the tracks on the flat plate profile on the edge noise of the tracks. According to the study, sawtooth geometries can reduce the noise level at high frequencies to 7-8 decibels [20]. In a study conducted on the numerical analysis of notches and using the DNS method, it was observed that the notches containing the flat plate-shaped sawtooth geometry added to the NACA 0012 profile reduce the tonal noise generated by the eddies at low frequencies and do not have a negative effect on the aerodynamic properties of the profile [21]. According to an experimental study conducted in 2010, the NACA 0012 airfoil was examined and compared with both sharp end marks edge geometry and sawtooth notches. In the study, it was observed that sawtooth notches change the amplitude of the tonal noise by changing the length of the separation bubble at the edge of the tracks [22]. In another study, the effect of sawtooth notches that are not in the form of flat plates on

6

noise, it was observed that both the broadband noise level was reduced and the tonal noise at low frequencies was eliminated [23].

Hansen et al. [5] were among the first researchers who experimentally examined the effect of leading-edge serration on acoustics. They observed that the tonal noise was reduced by 4-8 dB with the serrations created on the NACA0012 airfoil. Clair et al. [25] examined the effect of the sinusoidal serration structure of the leading edge of the NACA profile on the turbulence-blade interaction. According to the obtained results, the sound pressure levels decreased by 3-4 dB with the sinusoidal serration structure without adversely affecting the aerodynamic performance. Chaitanya et al. [26] is another group that experimentally examines the effects of serration amplitude and wavelength on aeroacoustic performance. According to the study, the serration amplitude is the most important parameter that dominates sound pressure levels. Miklosovic [27,28] studied the effect of whale fin geometry on aerodynamic performance. In this study, he investigated the stall performance of both serrated and non-serrated wing structures experimentally and found that wing serrations provide a 40% improvement in stall performance. The most important reason why serrated structures increase aerodynamic performance is the formation of blade tip vortices. Based on Miklosovic's [28] claim that aerodynamic improvement is achieved with the increase of blade tip vortices thanks to serrated structures, Stanway [29] changed the Reynolds number; aimed to analyze the interaction of tip vortices and serrations. Skillen et al. [30] experimentally demonstrated that with serrated airfoil structures, pressure gradients occur through the airfoil profile, and these structures cause secondary flow regions. Thanks to these high-energy secondary flow regions, the boundary layer energy level rises, which delays the boundary layer separation.

At the same time, in the 2000s, numerical studies have appeared to be made on reducing sound pressure levels with the serrated leading edge profile. Favier et al. [31] performed DNS (Direct Numerical Simulation) resolution at low Reynolds numbers for jagged geometries. Narayanan et al. [32] numerically investigated the effect of amplitude and wavelength of the serrations on acoustic characteristics. One of the most important parameters in noise control has been determined as the serration amplitude. The relationship between the serration amplitude and the noise level reduction in decibels was determined logarithmically. The reason for this logarithmic change has not been fully resolved by the researchers; however, it was observed that the noise control performance decreased as the amplitude increased. Rao et al. [33], in their

numerical study, observed that the serrated wing structure provides acoustic control by damping high-frequency eddies in the laminar-turbulent transition region.

Huang et al. [34] experimentally examined the effect of wavy leading edge blades in wind turbine applications. According to the results obtained, the serration structure delays the altitude loss. Lin et al. [35] are another research group, examines the effect of leading-edge and trailing-edge serration in horizontal wind turbines. They used the k-ω SST turbulence model in their work. It has been observed that the leading edge serration creates a higher traction force than the trailing edge serration. Wang et al. [36] are another research group argue that the application of the wavy structure to the vertical wind turbine blade has a positive effect on performance. It has been revealed as a result of the studies that the serrated structure delays the flow separation. Javaid [37] tried different geometries of serrations for gliders. The conical wing structure reduced the lift and increased the hydrodynamic balance.

Soderman et al. [38] investigated the effect of leading-edge serrated airfoil on performance numerically and experimentally. A study was conducted to determine the flow field and aerodynamic effects of serrations on a two-dimensional airfoil with Mach number 0.13. In the study performed with a model NACA 0066 and NACA0012 airfoil, the size of the serrations was found to be an important parameter. Smaller serrations (0.51 cm and below) created energizing eddies in the upper layer, resulting an increase in the angle of attack for maximum lift. Moreau and Doolan [39] investigated the effect of leading-edge and trailing-edge serration on the airfoil numerically and experimentally. The trailing edge serrations have been found to provide reductions in noise levels of up to 13 dB. It has been claimed that this is caused by eddy attenuation.

Wang et al. [40] investigated the effect of trailing edge serration on the airfoil using numerical and experimental methods. Experimental results show that noise is reduced in the frequency range of 1600-5000 Hz. The noise reduction in sound pressure level is 2 dB using the saw serrated trailing edge. As the free stream velocity increases, the noise-damping performance of the serrations decreases.

1.2 OBJECTIVE AND SCOPE OF THE THESIS

1.2.1 Problem

In the scope of this thesis, reduce the noise level by changing wavelength, amplitude and serration geometry. The sound pressure level is expected to fall around 60% in the literature. However, the goal of the thesis to reduce the sound pressure level of around 20%. Numerical and experimental studies are carried out . The numerical study are verified by experimental methodology.

1.2.2 Aim of The Thesis

The aforementioned literature review shows that although there is rapid growth in that field, understanding of the effect of the airfoil with a wavy leading edge on aeroacoustic and aerodynamic behaviour is still underdeveloped. In this thesis, the effects of serration geometry on turbulence-airfoil interaction and self-noise are examined both with experimental and numerical techniques. The main objectives of the research are given as follows:

✓ Revealing the flow characteristics around the wavy leading edge and underlying the mechanism of noise control.

✓ Examining the effect of the serration geometry, like wavelength and amplitude of the serration on the aeroacoustic performance of the NACA0012 profile.

✓ Understanding the effect of ınflow speed or Reynolds number on the level of noise reduction

✓ Quantifying the effect of angle of attack of serrated profile on aerodynamic performance

✓ To compare the noise reduction results of numerical and experimental study

In order to achieve these objects, experimental studies are conducted to investigate the noise radiation mechanisms of NACA0012 airfoil at a different angle of attacks, geometries and Reynolds numbers. Also, in order to visualize the flow field and capture the broadband nature of the noise sources and the damping mechanism, numerical studies are performed.

1.2.3 Design Parameters

The NACA0012 airfoil is used as a base profile with a chord length of c=150 mm and span the length of 300 mm. In order the examine the effect of serrations on performance smooth leading edge profile is modified to the wavy leading edge in the form of a sinusoidal profile with an amplitude, A, wavelength, λ, and chord length, c. Design parameters of the wavy leading edge used in the experiment and numerical studies are depicted in Table 1.2 The serration's amplitude and wavelength vary between 1.25< A<2.5 and 20<λ<60, respectively.

Table 1.2: Test Matrix

Configuration	A (mm)	λ(mm)	A/c	λ/c	λ/A	AOA (°)
Baseline	-	-	-	-	-	4,8,12,16
A1.25W20	1.25	20	0.008333	0.133	16	4,8,12,16
A1.25W30	1.25	30	0.008333	0.2	24	4,8,12,16
A1.25W60	1.25	60	0.008333	0.4	48	4,8,12,16
A1.875W20	1.875	20	0.0125	0.133	10.666	4,8,12,16
A1.875W30	1.875	30	0.0125	0.2	16	4,8,12,16
A1.875W60	1.875	60	0.0125	0.4	32	4,8,12,16
A2.5W20	2.5	20	0.016667	0.133	8	4,8,12,16
A2.5W30	2.5	30	0.016667	0.2	12	4,8,12,16
A2.5W60	2.5	60	0.016667	0.4	24	4,8,12,16

The corresponding Reynolds numbers are between $1x10^5$ and $3x10^5$, respectively. The angle of attack for each configuration is changed between 4°<aoa<16°. 40 configurations are tested in this study numerically. Serration amplitudes and wavelengths are non-dimensionalized by dividing by the chord length. The geometric parameters are shown in Figure 5.
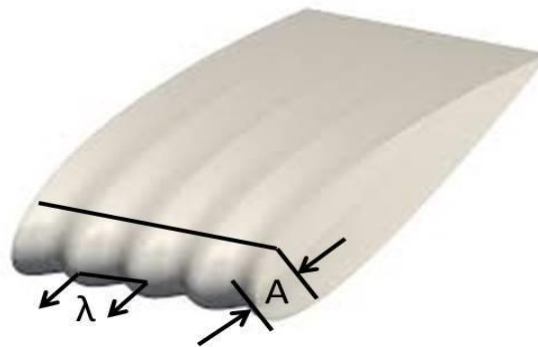
Figure 5: Geometric Parameters on Airfoil Profile

The wavy leading edge airfoil profile coordinated is defined using the Eq 1.1 defined in the Ref [31]. With the help of this formula, trailing edge coordination is kept constant, and the leading edge is stretched and contracted in line.

$$\begin{cases} y_{new} = y_{old} \\ x_{new} = \left(\frac{x_{old}}{x_{max}}\right)[x_{max} + (c(z) - c)] - [c(z) - c] \quad x_{old} < x_{max} \\ x_{old} \qquad\qquad\qquad\qquad\qquad\qquad\qquad x_{old} > x_{max} \end{cases} \qquad 1.1$$

Boundary conditions are selected as velocity inlet, pressure outlet.Naca profile defined as wall and it stands in the middle of the enclosure And the boundary conditions is given in Figure 6.
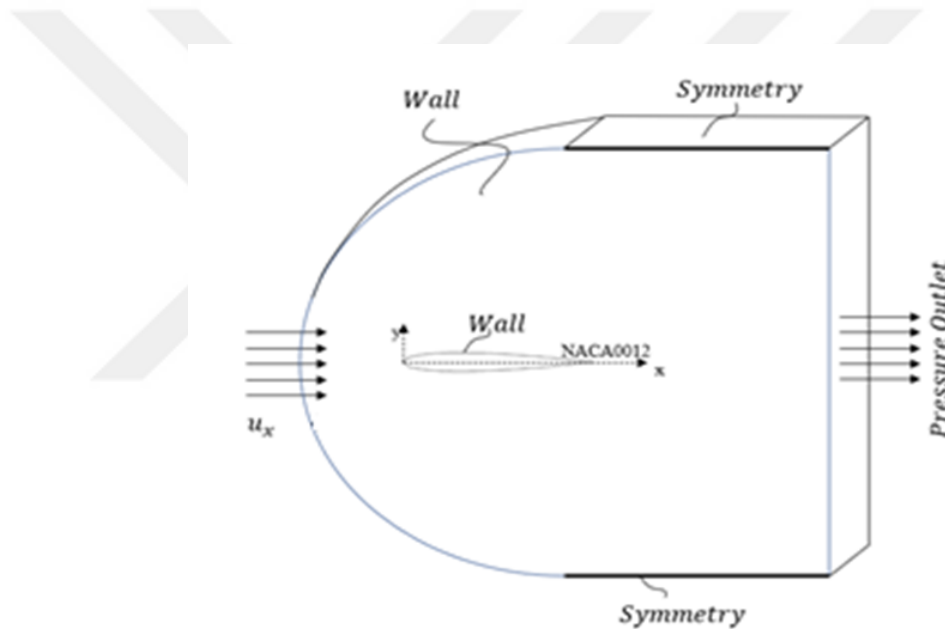
Figure 6: Boundary Conditions

2. THEORETICAL BACKGROUND

2.1 AERODYNAMIC PERFORMANCE OF AIRFOIL

With the change of the main profile, the aeroacoustic and aerodynamic effects on the wing also change depending on each other. The increase in aeroacoustic performance may have negative effects on aerodynamic performance due to the change in the airfoil. For this reason, it is aimed to determine the wing profile with optimum performance.

2.1.1 Flow Around airfoil

The configuration of the airfoil in tandem and the coordinate system are shown in Figure 7. The chord length of the symmetrical NACA 0012 airfoil, one of the basic airfoil geometries C.
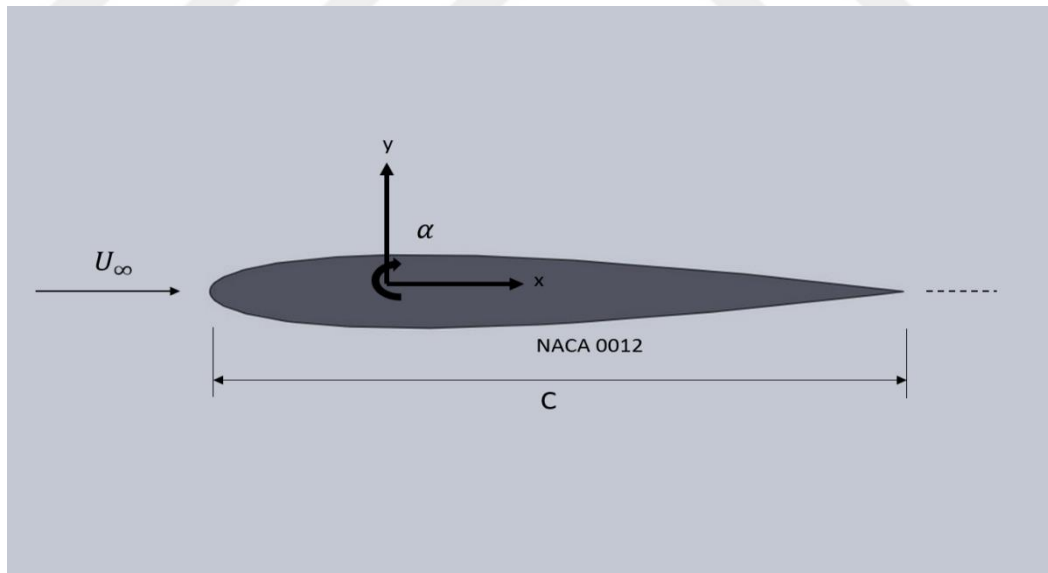
Figure 7: Flow configuration on a NACA 0012

2.1.2 Forces on Airfoil

The air in which the airfoil moves generates force, called lift and drag on its components. The resulting forces or force vectors are trigonometrically resolved to these lift and drag components perpendicular and parallel to the wind direction, respectively. Lift is the force that keeps the plane in the air and pushes it up. Drag force, on the other hand, is a force that acts in opposition to the relative motion of any object moving relative to a fluid. Drag force is the resistance that retards the forward motion of the aircraft. Therefore, the aircraft designer must achieve an airfoil that will produce high lift and low drag in the range of the aircraft's flight angles of attack. The force vectors on the airfoil are shown in the Figure 8.
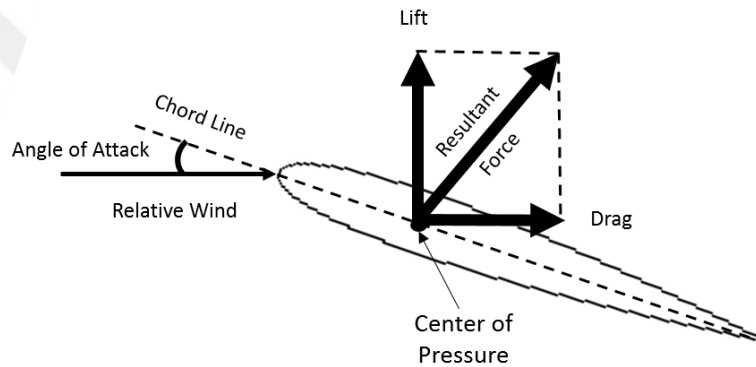
Figure 8: Force vectors on the airfoil

2.1.3 Blade Element Theory

Blade element theory is the application of standard blade theory to rotating theory. The blade is considered to be rigid at rotational speeds, so the largest force applied towards the blade is the centrifugal force, which is enough to keep the wing rigid. [41]. In vertical flight (including hover), the main complication is the need to integrate fundamental forces across the blade span. Compensating for this, useful simplification occurs, as the wing incidence and induced flow angles are normally small enough to allow small-angle approaches[42].

In cases where the flow is not stable, momentum theory cannot provide sufficient equations to solve for propeller thrust and torque at a given opening position. Blade element theory uses the geometric properties of the blade to determine the forces in the flow field. . Lift and drag force consists of the velocity of the flow above the blade.
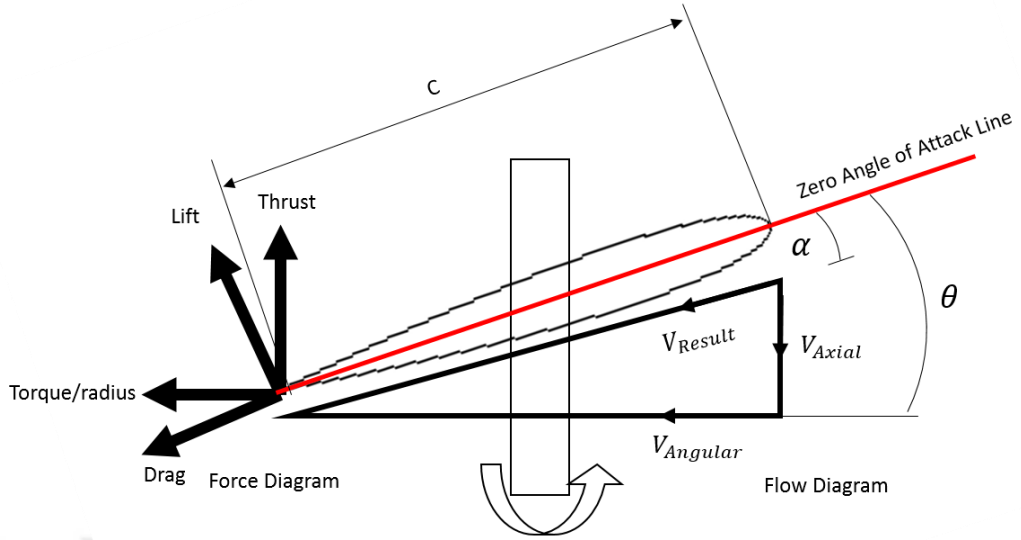
Figure 9: Blade Element Profile

Propeller thrust is calculated using these equations.

Lift Equation is,

$$\Delta L = C_L \frac{1}{2}\rho V_{Result}^2 c.\,dr \qquad\qquad 2.1$$

Drag Equation is,

$$\Delta D = C_D \frac{1}{2}\rho V_{Result}^2 c.\,dr \qquad\qquad 2.2$$

Change in thrust,

$$\Delta T = \Delta L cos(\emptyset) - \Delta D sin(\emptyset) \qquad\qquad 2.3$$

$$\Delta T = \frac{1}{2}\rho V_{Result}^2 C\big(C_L cos(\emptyset) - C_D sin(\emptyset)\big)Bdr \qquad\qquad 2.4$$

2.2 COMPUTATIONAL AEROACOUSTIC

Computational aeroacoustics is basically based on two methods. The first method is called DNS (Direct Numerical Analysis) and is based on solving compressible Navier-Stokes equations directly without the need for a turbulence model. This method, in which even the smallest turbulent structures can be solved, is not preferred because it is not suitable for today's processing power possibilities.

Another method is the LES (Large Eddy Simulation) model. Large eddy simulation methodology was used in this thesis. The reason for using this method the mesh structure used in this model acts as a kind of filter and completely resolves large-scale eddies, and analyzes small turbulent structures where the mesh is not sufficient by using scale models. Although it gives results close to the DNS method when the mesh criteria are met, it is much more efficient in terms of saving time.

The mesh structure to be used in CFD analysis is very important. The frequency band range of interest is directly based on cell sizes and solvent parameters. In general, it is aimed to place 20 cells for each wavelength in the area that is within the turbulent region, that is, in the area that creates the source of the noise. In other words, since the wavelength will decrease at high frequencies, the cell sizes will also decrease.

The frequency range to be examined also affects the solution time and time step. If a solution is desired at high frequencies, it is necessary to reduce the time step, and if a solution is desired at low frequencies, it is necessary to increase the total analysis time. For this reason, analysis times are very long in wide frequency ranges. As a general rule, the time step (T_s) and total analysis time (T_t) depending on the frequency range to be examined can be expressed as follows.

$$T_s = \frac{1}{10 * Max\ Frequency(Hz)}$$

2.5

$$T_t = \frac{20}{Min\ Frequency(Hz)}$$

Considering that the analyzes made within the scope of this thesis examine the range of 1000 Hz and 50000 Hz, it can be concluded that the time step to be used in the analyzes is $5x10^{-6}$ s, and the total analysis time is 0.02 s.

For turbulence solution in CFD analysis, using direct solution methods such as LES instead of turbulence modeling methods such as k-ε, k-ω, which are used together with RANS solution model, will give more suitable results especially for broadband analysis. If a study is carried out for narrow band rather than wide band (such as tonal noise detection), the use of time dependent URANS solution models can be considered.

In this thesis, considering the computational resources and time limitation, it was deemed appropriate to use the k-omega model. FW-H method was used for noise estimation.

2.2.1 Sound And Noise

The main focus of acoustics is on the study of erratic pressure variations that propagate in waves that can be perceived by the human ear. The human ear can detect pressure waves ranging from 20 Hz to 20 kHz.

Sound wave has frequency, length, period and velocity. The number of vibrations occurring in one second (can also be called the number of wave crests per second) is called the frequency of the sound. The unit of frequency is Hertz (Hz). Wavelength is the length of the wave that makes up the sound wave. It can be considered as the distance between two wave crests or two wave troughs. Sound pressure is a pressure fluctuation at a point. The time-dependent expression of instantaneous sound pressure in total pressure is given as follows:

$$P_{(top)}(t) = p(t) + P_{(static)}(t) \qquad 2.6$$

Here, both terms on the right side of the equation are functions of time. But the changes on static pressure are much slower. Therefore, it is generally considered to be constant. The effective sound pressure is obtained by taking the root mean square (RMS) of the time-dependent pressure data. The speed of sound in air, c, can be calculated with the following equation, depending on the density of the medium:

$$c = \sqrt{\frac{\gamma p_{static}}{\rho_{static}}} \qquad 2.7$$

Here, $P_{(static)}$ is the static pressure value, ρ_{static} is the static average density value, and γ is the heat capacity ratio. For air, the sound velocity function can simply be expressed by the following equation, depending on the temperature (t °C):

$$c = 331.4 + 0.607 * t \qquad 2.8$$

The speed of sound is usually 340 m/s for 15°C at sea level. The propagation of sound under water varies according to temperature, salinity and depth. The speed of

sound under water is 4.3 to 4.4 times that in air. The speed of sound is considered to be about 1500 m/s for underwater. The ratio of the instantaneous velocity to the reference sound velocity is expressed as a dimensionless coefficient, the Mach number:

$$Ma = \frac{v}{c} \qquad 2.9$$

Situations where the Mach number is greater than 1 are defined as supersonic stream. Supersonic flows can be classified as nonlinear for the acoustic research field, similar to current noise. The sound pressure level (SPL) defines the level humans hear and is measured using the unit dB. It is defined as follows:

$$SPL = 20log_{10}\frac{p_{rms}}{p_{ref}} = 10log_{10}[\left(\frac{p_{rms}}{p_{ref}}\right)^2 \qquad 2.10$$

The reference pressure value used in Equation 2.10 is accepted as 2x10-5 Pa for air and 10-6 Pa for other environments. 2x10-5 Pa is the lower hearing threshold of the human ear and corresponds to 0 dB. Another methodology used to express the sound level is the sound power level. Similarly, the sound power level is measured using the dB unit and is defined as follows:

$$dB = 10log_{10}(\frac{P_1}{P_2}) \qquad 2.11$$

Here, P_1 represents the measured power value and P_2 represents the reference power value. The reference power value is accepted as 10^{-12}W in most countries. The dB measure should not be considered as a unit similar to length or mass units. dB is just a level measure that tells us where we are relative to a reference value and it should be noted that it scales logarithmically. Scaling logarithmically actually makes differences of the order of 10 powers 27 appear small as numerical values.

It is also possible to add n different sound levels with the addition expression in the logarithmic expression given in Equation 2.12:

$$dB = 10log_{10}\left(10^{\frac{SPL1}{10}} + 10^{\frac{SPL2}{10}} ... + 10^{\frac{SPLn}{10}}\right) \qquad 2.12$$

2.2.2 Sound and Noise Fundamentals

In this section, the effects of the q function, which is the three different components of the volume integration, on the $p - p_0$ pressure area are given.

$$q = q_1 + q_2 + q_3 \qquad 2.13$$

The three components given in equation 2.13 help us to express point sources of noise that cause noise generation aerodynamically. These sources are called monopole, dipole and quadrupole sources. These three types of point sources transfer kinetic energy to acoustic energy in three different ways.

2.2.2.1 Monopole, Dipole And Quadrupole Sources

The pressure variations created by the volume integrals over [q1]/4πr are expressed by the following equation:

$$p - p_0 = \frac{1}{4\pi} \int_V \frac{1}{r} \left[\frac{\partial M}{\partial t}\right] dV \qquad 2.14$$

Starting from the formula given in equation 2.14, the propagation equation for a monopole source can be obtained in the following form:

$$p_M - p_0 = \frac{\omega \rho_0 Q}{4\pi} \frac{f(t - \frac{r}{c_0})}{r} \qquad 2.15$$

The pressure variations created by the volume integrals over [q2]/4πr are expressed by equation 2.15:

$$p - p_0 = \frac{1}{4\pi} \int_V \frac{1}{r} \left[\frac{\partial F_i}{\partial y_i}\right] dV \qquad 2.16$$

Starting from the formula given in Equation 2.16, the propagation equation for the dipole source can be obtained in the following form.

$$p_D - p_0 = \frac{\omega \rho_0 Q h \cos \vartheta}{4\pi} \lim_{\Delta r \to 0} \left(\frac{g(t, r + \Delta r) - g(t, r)}{\Delta r}\right) = \frac{\omega \rho_0 h Q}{4\pi} \cos \vartheta \frac{\partial}{\partial r} g(t, r) \qquad 2.17$$

Here, the D subscript for pD represents the dipole source term. The pressure variations created by the volume integrals over [q3]/4πr are expressed by the following equation:

$$p - p_0 = \frac{1}{4\pi} \int_V \frac{1}{r} \left[\frac{\partial^2 F_i}{\partial y_i \partial y_j} \right] dV \qquad 2.18$$

Starting from the formula given in equation 2.18, the propagation equation for a monopole source can be obtained in the following form:

$$r_1 \rightarrow r$$

$$r_2 \rightarrow r + \Delta r; \ \Delta r = -l\cos\vartheta \ (for \ l \rightarrow 0)$$

$$p_K - p_0 = \frac{\omega \rho_0 M l \cos\vartheta}{4\pi} \lim_{\Delta r \rightarrow 0} \frac{1}{\Delta r} \left(\frac{x_1 - 1 - y_1}{r + \Delta r} \frac{\partial}{\partial(r + \Delta r)} g(t, r + \Delta r) \right) - \frac{x_1 - y_1}{r} \frac{\partial}{\partial r} g(t, r) =$$

$$\frac{\omega \rho_0 M l}{4\pi} \cos\vartheta \frac{\partial}{\partial r} \left(\cos\vartheta \frac{\partial g}{\partial r} \right) \qquad 2.19$$

The power expressions of the dipole and quadrupole source terms are as follows:

$$\prod_D \infty \frac{F_i^2}{\rho_0} \frac{\omega^2}{c^3}$$

$$2.20$$

$$\prod_K \infty \frac{T_{ij}^2}{\rho_0} \frac{\omega^4}{c^5}$$

Lighthill accepted in his studies that the frequencies (ω) of the sources are proportional to U_∞ / l, and that the term T_{ij} is proportional to $\rho_0 U_\infty^2$ [43].where U_∞ is the mean circumferential velocity and l is the turbulence correction distance.

He accepted in his studies that the Curle Fi term is proportional to $\rho_0 U_\infty / l$ [44]. Substituting these expressions in equation 2.20, omitting l, we obtain the following equations for the total acoustic power expression of the dipole and quadrupole source types:

$$\prod_D \infty \rho_0 \frac{U_\infty^6}{c^3}$$

$$2.21$$

$$\prod_K \infty \rho_0 \frac{U_\infty^8}{c^5}$$

For the quadrupole term, it is seen that the speed expression of the noise originating from the turbulence in the open flow is the eighth power and the sound velocity expression is the fifth power. The most famous conclusion to emerge from Lighthill's work is this statement, and it has been proven experimentally many times over.

The point to be noted here is that the acoustic power expression of the dipole source term is the sixth power of the velocity, and the sound velocity expression is the third power. This means that loading noise is much more effective than turbulent noise at low speeds. From this, it can be deduced that the loading noise originating from on-vehicle moorings will be the dominant aeroacoustic source at speeds lower than 200 km/h.

In summary, the noise created by turbulent structures is equal to the volumetric distribution of quadrupole sources, and the acoustic efficiency of quadrupole sources is quite poor compared to monopole and dipole sources. Curle showed that the noise field emitted from a rigid surface located near the turbulence region is equal to the dipole sources distributed over the surface, and the noise emitted from the dipole sources is acoustically much more effective than the turbulent structures [45].

2.2.3 Aeroacoustic Analogy

The historical development of the Ffowcs Williams Hawkings analogy used to get acoustic solutions in the thesis is given. Equations that started with Lighthill analogy and then developed by curle and obtained lastly by Ffowcs Williams Hawkings are mentioned.

2.2.3.1 Lighthill Analogy

Lighthill developed the idea of distributing the source (monopole, dipole, and quadrupole) over the surface and volume as it transitions from turbulent flow to acoustics [46] The continuity equation and momentum conservation equation for compressible flows are expressed as:

$$\frac{\partial \rho}{\partial t} + \frac{\partial \rho v_i}{\partial x_i} = 0 \qquad\qquad 2.22$$

$$\frac{\partial \rho v_i}{\partial t} + \frac{\partial \rho v_i v_j}{\partial x_j} = \frac{\partial \rho}{\partial x_j} + \frac{\partial \tau_{ij}}{\partial x_j} \qquad\qquad 2.23$$

Here τ_{ij} denotes the viscous stress tensor and its expansion is as follows:

$$\tau_{ij} = \mu \left(\frac{\partial v_i}{\partial x_j} + \frac{\partial v_j}{\partial x_j} - \frac{2}{3} \frac{\partial v_k}{\partial x_k} \delta_{ij} \right) \qquad 2.24$$

Taking the derivative of equation 2.22 with respect to time together with the divergence of equation 2.23 yields a single expression:

$$\frac{\partial^2 \rho}{\partial t^2} - \frac{\partial^2 \rho v_i v_j}{\partial x_i x_j} = -\frac{\partial}{\partial x_i} \left(-\frac{\partial \rho}{\partial x_j} + \frac{\partial \tau_{ij}}{\partial x_j} \right) \qquad 2.25$$

Equation 2.26 is obtained if equation 2.27 is arranged with the chain rule and the kronecker delta function (δ_{ij}).

$$\frac{\partial^2 \rho}{\partial t^2} = \frac{\partial^2}{\partial x_i x_j} (\rho v_i v_j + \rho \delta_{ij} - \tau_{ij}) \qquad 2.26$$

$$c_\infty^2 \frac{\partial^2 \rho}{\partial x_i^2} - \frac{\partial^2 p \delta_{ij}}{\partial x_i x_j} = 0 \qquad 2.27$$

Equation 2.28 needs to be subtracted from equation 2.26 to obtain the Lighthill equation. This also gives the expression for the inhomogeneous wave equation:

$$\frac{\partial^2 \rho}{\partial t^2} - c_\infty^2 \frac{\partial^2 \rho}{\partial x_i^2} = \frac{\partial^2 \tau_{ij}}{\partial x_i x_j} \qquad 2.28$$

The Lighthill equation contains the wave operator and the noise source term on the left side of the equation. On the right side of the equation, it contains the Lighthill stress tensor (τ_{ij}). The Lighthill stress tensor is defined as:

$$\tau_{ij} = \rho v_i v_j - \tau_{ij} + (p - c_\infty^2 \rho) \delta_{ij} \qquad 2.29$$

Here, τij defines the noise generated by viscous forces, $\rho v_i v_j$ the Reynolds stress term, $(p - c_\infty^2 \rho)\delta_{ij}$ the nonlinear behavior in the noise generation. When we look at the region outside the turbulence zone, the static situation is explained by the terms ρ_∞, p_∞, and $c_\infty{}^2$, . In a region outside the variable turbulent region, the concept of noise is expressed by locally occurring fluctuations (').

$$\rho = \rho_\infty + \rho'$$

$$p = p_\infty + p'$$

2.30

The expression homogeneous wave equation allows us to write equation 2.29 as an inhomogeneous wave equation using density fluctuations terms:

$$\frac{\partial^2 \rho'}{\partial t^2} - c_\infty^2 \frac{\partial^2 \rho'}{\partial x_i^2} = \frac{\partial^2 \tau_{ij}}{\partial x_i x_j}$$

2.31

For the above expression, the term Lighthill stress tensor turns into the following form [46]:

$$\tau_{ij} = \rho v_i v_j - \tau_{ij} + (p' - c_\infty^2 \rho') \delta_{ij} - \tau_{ij}$$

2.32

In this case, the fact that the terms on the left side of the equation describing the wave are not balanced means that the term Tij changes rhythmically, which generally occurs within the turbulent region. It is theoretically possible to obtain exact solutions from the Lighthill equations, but for this it is necessary to know the flow field at each point in each time step. When trying to solve equation 2.28 for an infinite solution space, it is necessary to use the free space Green's integration for the density fluctuation term together with the delayed time step term.

$$\rho'(x,t) = \frac{1}{4\pi c_\infty^2} \frac{\partial^2}{\partial x_i \partial x_j} \int_V \left[\frac{T_{ij}}{r} \right] dy$$

2.33

Here y represents the source location and x represents the observer location. It can be seen from this expression that the four separate source areas are extremely close to each other. The Lighthill analogy defines the quadrupole field. Another way to see this situation is to use distributed quadrupoles. In order to do this, it is necessary to make use of mathematical correction functions (convolution products) when converting spatial concepts to time derivatives. As a result, Lighthill's integral formulation is obtained.

$$\rho'(x,t) = \frac{1}{4\pi c_\infty^2} \frac{\partial^2}{\partial x_i \partial x_j} \int_V \frac{1}{r} \left[\frac{\partial^2 T_{ij}}{\partial y_i \partial y_j} \right] dy$$

2.34

22

2.2.3.2 Curle Analogy

The Curle analogy is an extended version of the Lighthill analogy created by Curle based on the Lighthill analogy. Curle obtained the definition of dipole-induced noise generation by including the flow-body interaction in the Lighthill analogy [47] This method is realized by incorporating mathematical control surfaces into the system. Similarly, free space Green's functions are used here as well. Instead of the term pressure (p'), density (ρ') is used as an aeroacoustic variable. The force field density of the expression given in equation 2.31 is as follows:

$$\frac{\partial^2 \rho'}{\partial t^2} - c_\infty^2 \frac{\partial^2 \rho'}{\partial x_i^2} = \frac{\partial^2 \tau_{ij}}{\partial x_i x_j} - \frac{\partial f_i}{\partial x_i} \qquad 2.35$$

Lighthill's inhomogeneous wave equation can be evaluated by considering many general theories. One of them is the Kirchoff formulation, and the following expression was obtained in this way:

$$\rho' = \rho - \rho_0 \frac{1}{4\pi c_\infty^2} \int_V \frac{\partial^2 \tau_{ij}}{\partial y_i \partial y_j} \frac{\partial y}{|x-y|} + \frac{1}{4\pi} \int_S \left\{ \frac{1}{r}\frac{\partial p}{\partial n} + \frac{1}{r^2}\frac{\partial r}{\partial n}\rho + \frac{1}{c_\infty r}\frac{\partial r}{\partial n}\frac{\partial \rho}{\partial t} \right\} dS(y)$$
$$2.36$$

It should be noted here that the equation gives instant results with the delayed time step and the r distance is calculated with the $|x - y|$ term. It can be seen that the above expression becomes Lighthill integration if the surface integral term is neglected. If the volume integral term is diverged twice and the T_{ij} tensor is put in place, the following expression is obtained for fixed surfaces (not moving in their normal direction):

$$\rho - \rho_0 = \frac{1}{4\pi c_\infty^2}\frac{\partial}{\partial x_i x_j} \int_V \frac{T_{ij}}{r} dy - \frac{1}{4\pi c_\infty^2}\frac{\partial}{\partial x_i} \int_S \frac{P_i\left(y, t-\frac{r}{c_\infty}\right)}{r} dS(y)$$
$$2.37$$

Here

$$P_i = -n_j p_{ij} = -n_j\left(p\delta_{ij} - \tau_{ij)}\right) \qquad 2.38$$

equality exists. As a result, the Curle formulation is obtained as follows:

$$\rho'(x,t) = \frac{1}{4\pi c_\infty^2} \frac{\partial^2}{\partial x_i \partial x_j} \int_V \frac{T_{ij}}{r} dy - \frac{1}{4\pi c_\infty^2} \frac{\partial}{\partial x_i} \int_S \frac{P_i\left(y,t-\frac{r}{c_\infty}\right)}{r} dS(y)$$

<div align="right">2.39</div>

The curl analogy can be used to estimate dipole noise from fixed surfaces. This analogy, which can also be used in time-independent analyses, allows us to see the noise levels created by the surfaces before proceeding with the time-dependent analysis and to make the necessary mesh structure improvements. Curle analogy can be used with the RANS method and turbulence models developed for RANS.

2.2.3.3 FFowcs Williams and Hawkings Equations

Ffowcs Williams and Hawkings extended the acoustic equations to consider solid boundaries. FW-H (Ffowcs Williams Hawkings) integral equations are used in the aeroacoustic calculation part of the method. These equations uses the transient flow features from the CFD simulation and calculates the far-field airfoil noise at the observer location.[48] The FW-H code is validated by comparing the farfield results of a source's estimation and analytical solution.

After several mathematical arrangements the final equation yields as:

$$\rho(x,t) - \rho_0 = \frac{1}{4\pi c_\infty^2} \frac{\partial^2}{\partial x_i \partial x_j} \int_V \frac{T_{ij}'^*}{r\left(1-\frac{l_j v_j}{c_\infty}\right)} dV(y^*) - \frac{1}{4\pi c_\infty^2} \frac{\partial}{\partial x_i} \int_V \frac{F_i^*}{r\left(1-\frac{l_j v_j}{c_\infty}\right)} dS(y^*) +$$

$$\frac{1}{4\pi c_\infty^2} \frac{\partial}{\partial t} \int_S \frac{Q^*}{r\left(1-\frac{l_j v_j}{c_\infty}\right)} dS(y^*)$$

<div align="right">2.40</div>

$$T_{ij}'^* = \rho(u_i^* + v_i)(u_j^* + v_j) - \tau_{ij}^* + (p - c_\infty^2(\rho - \rho_\infty))\delta_{ij}$$
$$F_i^* = (\rho(u_i^* + v_i)u_j^* + p\delta_{ij} - \tau_{ij}^*)n_j$$
$$Q^* = (\rho_\infty v_i + \rho u_i^*) n_i$$

<div align="right">2.41</div>

$T_{ij}'^*$ is formed by the fluctuating stresses in the fluid and represents the quadrupole sources.

F_i^* represents the dipole sources due to fluctuating sources on the surface.

$Q^*\ast$ is the monopole sources which is comprised by the fluctuating mass fluxes through the surface.

u_i^* becomes 0 for impermeable surfaces so the dipole sources reduce $F_i^* = (p\delta_{ij} - \tau_{ij}^*)n_j$ monopole sources to $Q = (\rho_\infty v_i n_i)$.

The FW-H method is used as an aeroacoustic calculation tool in many CFD commercial codes used today. The mathematical expressions used in the method have been tried to be given as a summary. The FW-H method was used for the estimation of the far-field noise in the current noise calculations around the airfoil in this study.

2.3.Fast Fourier Transform

The algorithm for converting time-dependent data into frequency very quickly is called FFT (Fast Fourier Transform). In general, vibration analysis is used to compare the frequency and intensity of the mixed signals received according to time and the amplitudes of the signals according to the frequency. Since noise is a kind of vibration data, it is suitable for FFT use.

The Fourier transform at frequency ω is represented by the function:

$$X(\omega) = \frac{1}{\sqrt{2\pi}} \int_{-\infty}^{\infty} x(t)e^{-iwt}dt \qquad 2.42$$

Here t is time (second) and ω is angular frequency (radian second). Substituting ω=2πf for the angular frequency expression gives the following expression:

$$X(\omega) = \frac{1}{\sqrt{2\pi}} \int_{-\infty}^{\infty} x(t)e^{-i2\pi ft}dt \qquad 2.43$$

Applying the inverse transformation to this expression gives the following equation:

$$X(\omega) = \frac{1}{\sqrt{2\pi}} \int_{-\infty}^{\infty} x(f)e^{-i2\pi ft}df \qquad 2.44$$

According to FFT, all complex signals are actually composed of simple harmonics. Non-repeating signals are ignored in the Fourier transform. Periodic ones are separated from complex signals and separated into harmonics.

3. NUMERICAL METHODS

CFD analyzes applied to airfoils and aiming to find pressure fluctuations on the body surface are based on solving RANS (Reynolds-Averaged-Navier-Stokes) equations by using finite volume extraction, pressure correction and SST k-ω turbulence model. In addition, the k-omega method was also used in an analysis. In this section, brief information is given about the mentioned concepts, methods and models.

3.1 REYNOLDS-AVERAGED NAVIER STOKES EQUATIONS (RANS EQUATIONS)

Approximate and simplified solutions of the Navier-Stokes equations are sought in order to reveal the average properties of turbulence by constraining the spatial and temporal scales. One of the modeling that provides the realization of the mentioned analysis is the RANS-based modeling type. In Equation 3.1 expressed below, all scales except organized structures are modeled. This equation, in which the time derivative is also added, can also be called URANS (Unsteady Reynolds-Averaged Navier-Stokes).

$$\frac{\partial U_i}{\partial t} + \frac{\partial U_j U_i}{x_j} = -\frac{1}{\rho}\frac{\partial P}{\partial x_i} + \frac{\partial}{\partial x_j}(2\vartheta S_{ij} - \overline{U_i' U_j'}) \qquad 3.1$$

The term $\tau_{ij} = -\overline{U_i' U_j'}$ is Reynolds stress tensor.

S_{ij} term is mean strain stress-rate tensor,

$$S_{ij} = \frac{1}{2}(\frac{\partial u_i}{\partial x_j} + \frac{\partial u_j}{\partial x_i}) \qquad 3.2$$

3.2 FINITE VOLUME DISCRETIZATION

Navier-Stokes equations or other equations used for solution need to be discretized in order to be converted into equations that can be solved numerically.

The discretization process can be expressed in terms of finite elements, finite differences or finite volume methods in which calculations can be made.

It is possible to obtain the transport equations modeling the fluid in the form of conservative differential equations by considering a fixed infinitesimal element in space and calculating the momentum transfer on all surfaces of this element.

Finite volume discretization is based on integrating these equations across a finite volume. In the Cartesian tensor notation of the convection and diffusion convection equation of a convection property (eg. temperature) of the flow, such as φ,

$$\rho \frac{\partial \phi}{\partial t} + \rho \frac{\partial (U_j \phi)}{x_j} = \frac{\partial}{\partial x_j}\left(\Gamma \frac{\partial \phi}{\partial x_j}\right) + S \qquad 3.3$$

can be expressed as discretization process. Here; U denotes velocities in three directions, φ any transport property of the flow, Γ the diffusion coefficient, and S the source term. If the equation is written in permanent and one-dimensional form, in order to obtain a plain and as simple equation form as possible,

$$\rho \frac{d(U\phi)}{dx} = \frac{d}{dx}\left(\Gamma \frac{d\phi}{dx}\right) + S \qquad 3.4$$

equation is obtained.

3.3 LARGE EDDY SIMULATION (LES) MODEL

DNS (Direct Numerical Solution) modeling is not required due to limited time and processing power. Instead, turbulent eddies can be resolved directly. However, it is not practical for high Reynolds number flows. On the other hand, RANS is not a method that can resolve large eddies. The LES model allows us to get the right solution without using the RANS and DNS models. Large eddy simulation is a combination of the direct resolution of large eddies and the resolution of small eddies via the Subgrid-scale model (SGS)[20]. The advantage of LES is its ability to dissolve large eddies. Large eddies occur at high angles of attack when simulating airfoils. With the increase in the number of meshes, it requires a lot of processing power to solve this model. For these advantages, LES was chosen as the most suitable method for the problem.[49]

The unsteady Navier stokes equations are filtered to obtain the equations of the large eddy simulation. FLUENT uses filtering through finite volume discretization.

Navier-Stokes equations;

$$\frac{\partial u_i}{\partial x_i} = 0 \qquad\qquad 3.5$$

$$\frac{\partial u_i}{\partial t} + \frac{\partial}{\partial x_i}(u_i u_j) = -\frac{1}{\rho}\frac{\partial P}{\partial x_i} + \frac{\partial}{\partial x_j}\left(\frac{\mu}{\rho}\sigma_{ij}\right) - \frac{\partial \tau_{ij}}{\partial x_j} \qquad\qquad 3.6$$

Here, σ_{ij} is the stress tensor which reads,

$$\sigma_{ij} = \left(\frac{\partial u_i}{\partial x_j} + \frac{\partial u_j}{\partial x_i}\right) - \frac{2}{3}\delta_{ij}\frac{\partial u_l}{\partial x_l} \qquad\qquad 3.7$$

Where τ_{ij} is subgrid scale stress. τ_{ij} is unknown and need to be modeled.

$$\tau_{ij} = \overline{u_i u_j} - \overline{u_i}\,\overline{u_j} \qquad\qquad 3.8$$

FLUENT gives us,

$$\tau_{ij} - \frac{1}{3}\tau_{kk}\delta_{ij} = -2\mu_t \overline{S_{ij}} \qquad\qquad 3.9$$

The μ_t term is defines eddy viscosity at SGS, Other term τ_{kk} isotropic definition of subgrid scale stresses and Mean strain tensor is similar to RANS eq 3.2 Eddy viscosity is defined in Smagorinsky-Lilly subgrid-scale modelling,[50]

$$\mu_t = \rho L_S^2 |\overline{S}| \qquad\qquad 3.10$$

$$|\overline{S}| = \sqrt{2\overline{S_{lj}S_{lj}}} \qquad\qquad 3.11$$

And L_S is the mix length of the subgrid scales,

$$L_S = \min(\kappa d, C_S V^{\frac{1}{3}}) \qquad\qquad 3.12$$

The von karma constant is symbolized by κ. d is symbolized as the nearest wall distance.. Also, n Fluent, the smagorinsky constant is represented as C_S with a value of 0.1. Finally, V symbolizes the volume of the calculation cell. [51]

28

4. DEVELOPMENT OF COMPUTATIONAL MODEL AND VALIDATION STUDY

Numerical operating conditions are presented in Table 4.1. In assigning the attack angle values to the profile, instead of changing the profile of the profile relative to the air, the method of sending the air at an angle to the profile, which provides convenience in terms of drawing and creates the same conditions, is used.

Table 4.1: Numerical Simulation Parameters

Turbulent Kinetic Energy	1.2043 kg/m^3
Freestream Velocity	15 m/s
Angle of Attack (aoa)	4,8,12,16,20
Turbulent Kinetic Energy	4.184 m^2/s^2
Dissipation rate	2.77 1/s
Chord Length	0.15 m
Span Length	0.06 m
Reynolds Number	1.5x10^5

4.1 GEOMETRY AND MESH STRUCTURE

The NACA 0012 profile used in this study is preferred because it is widely used in the field of aerodynamics and many experimental and numerical studies have been carried out on this profile. The comparison of the values used in the calculations was compared with the technical report prepared by NASA. The geometry of the NACA0012 profile used in the calculations was created by combining the points on the coordinate plane.The length of the profile was determined as 0.15 m to match the technical report. Also quadrilateral cells are used for this URANS simulation because they generate less numerical diffusion than triangular cells. The formula used in the creation of the NACA 0012 geometry used in the calculations is expressed by equation 4.1 The geometry of the profile can be seen in Figure 10 in general.

$$y_t = \frac{5t}{c\left[0.2969\sqrt{\frac{x}{c}} - 0.1260\left(\frac{x}{c}\right) - 0.3516\left(\frac{x}{c}\right)^2 + 0.2843\left(\frac{x}{c}\right)^3 0.1015\left(\frac{x}{c}\right)^4\right]} \qquad 4.1$$

In the equation, c is the length of the profile, x is a position between 0 and c on the profile, y_t is the half thickness at any x value, and t is the maximum thickness on the profile.
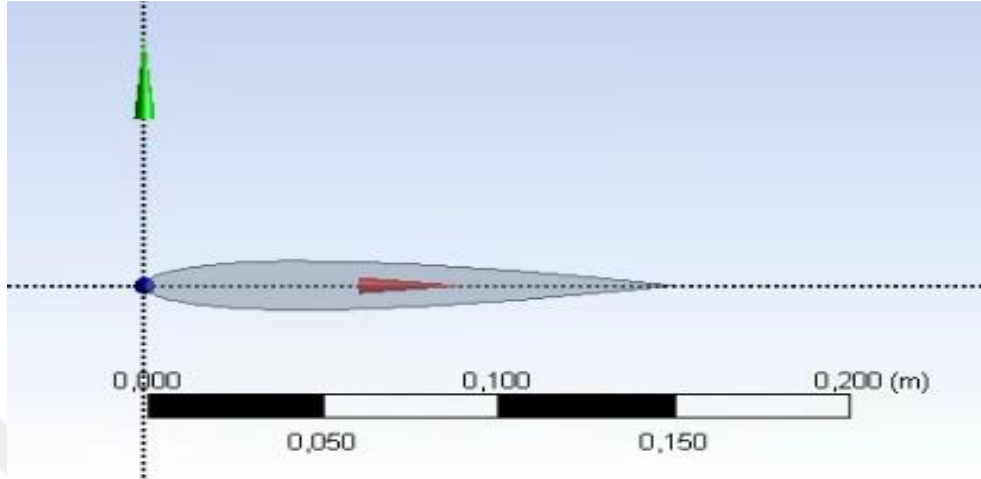

Figure 10: Naca0012 Profile Geometry

In this study 3D C Type meshing method is selected for grid structure. It is aimed to minimize numerical errors by meshing more frequently towards the region where the boundary profile is located. The mesh models are created in such a way that the value representing the dimensionless distance from the wall is approximately y +=1 in order to analyze the boundary layer in the best way. C type mesh structure is shown in Figure 11 and Figure 12.
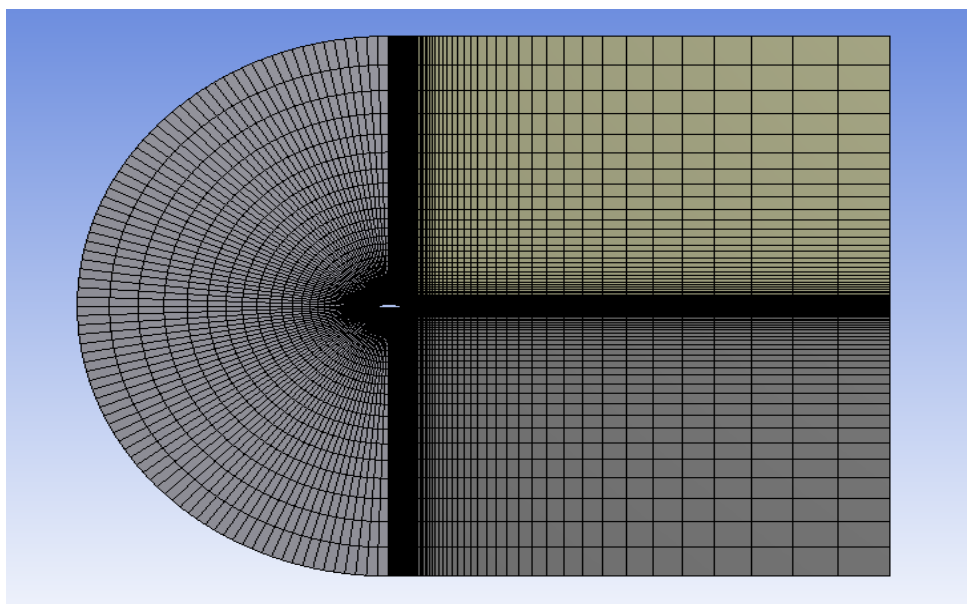

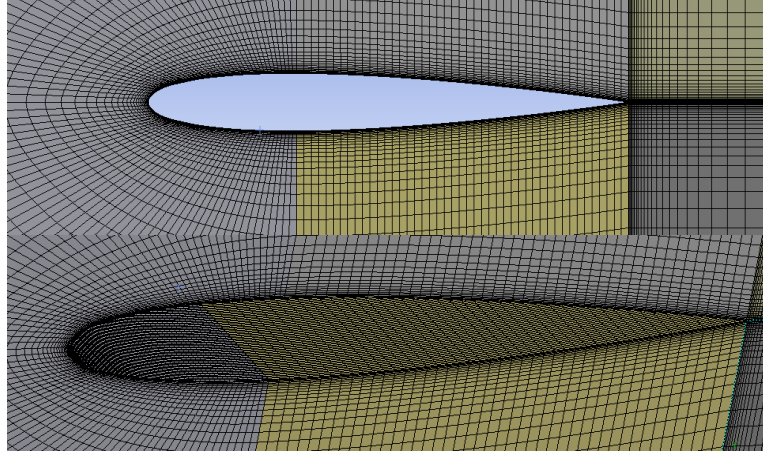
Figure 11: 3D C Type Mesh Structure

Figure 12: C Type Mesh Structure Near the Profile

4.2 MESH INDEPENDENCY STUDY

Due to the complexity of the geometry, the mesh structure was created by dividing into 4 different mesh zones as depicted in Figure 10. The hexahedral mesh structure, which is more preferred in external flow analyses and gives more consistent results with the experimental data, is preferred. The mesh structure is tightened around the airfoil with the distance from the airfoil surface to the nearest grid point fixed y+<5.

To obtain results that are independent form the mesh, it is expected that the results of the Computational Fluid Dynamics (CFD) simulations will not change with the mesh structure. As it becomes independent from the mesh structure, the solution becomes continuous, and discretization errors are minimized. As, Chen et al. [24] claimed that, the hardest case to achieve mesh independency for wavy profiles is the geometry with largest amplitude and smallest wavelength, mesh sensitivity study is performed for A2.5W20 airfoil as it has the largest amplitude and smallest wavelength. For angle of attack 4°, CD and CL variations are depicted for the different number of mesh elements in Table 4.2. The lift coefficient and drag coefficient of an airfoil are defined by

$$C_L = \frac{F_L}{\frac{1}{2}\rho u^2 A} \qquad\qquad 4.2$$

$$C_D = \frac{F_D}{\frac{1}{2}\rho u^2 A} \qquad\qquad 4.3$$

The results of the mesh independency study are given in Table 4.2 for the 4° angle of attack. According to the obtained results, the differences after fine mesh between two mesh structures reduced to lower than 0.04%. Considering the

31

computational cost, it is decided to use a network structure with $4x10^6$ elements in future studies.

Table 4.2: Mesh sensitivity study

	Total nodes	Lift Coefficient	Drag Coefficient	ΔCL	ΔCD
Coarse Mesh	$2x10^6$	0.4512	0.0246	-	-
Medium Mesh	$2.5x10^6$	0.4614	0.0249	2.2 %	1.2 %
Fine Mesh	$4x10^6$	0.4618	0.0251	0.08%	0.79%
Very Fine Mesh	$5x10^6$	0.4620	0.02518	0.04%	0.3%

4.3 . VALIDATION STUDY

In the validation study to ensure the reliability of the method used in CFD calculations, the analyzes of the NACA 0012 profile at three different angles of attack were performed and the Lift coefficients (C_L) were compared as output. C_L formulation given in Equation 4.2.Comparison of C_L values with NASA experiments with same Reynolds Number is given in Table 4.3.

Table 4.3: Validation Study Results

AoA(°)	CFD C_L	Experiment C_L	Error(%)
0	0	0	0
10	1.0533	1.0778	2.32
15	1.4869	1.5068	1.33

As can be seen in Table 4.3, the maximum margin of error is around 2.3, which is considered negligible.

4.4 GEOMETRICAL PARAMETERS

Sinusoidal waves are prepared with Matlab code with selected parameters that are placed on the leading edge of the original naca profile. A serrated airfoil structure was created by placing the maximum thickness of the naca profiles on top of these waves in 3 different compartments. These 3 different positions are the start, middle and peak of the sinusoidal wave.
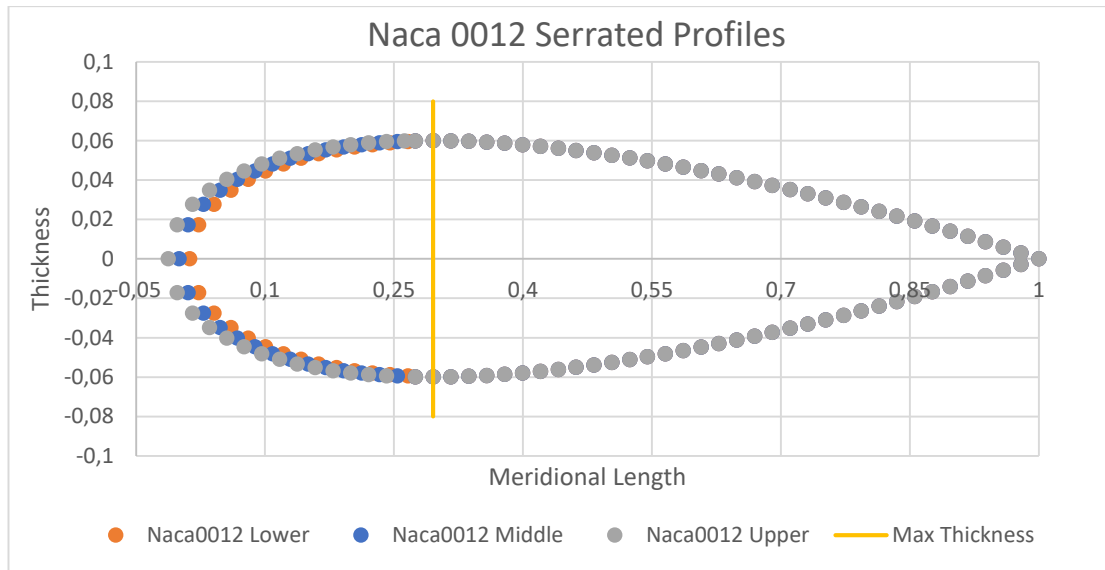
Figure 13: Diagram of the Naca Profile on a Sinusoidal Wave

The numerical values of the parameters used are shown in

Table 4.4

Table 4.4: Geometric Parameters Values

Case No	h (mm)	λ (mm)	h/c	λ/c	λ/h	AoA(°)
1	1.25	20	0.00833	0.13333	16	4
2	1.25	30	0.00833	0.2	24	4
3	1.25	60	0.00833	0.4	48	4
4	1.25	20	0.00833	0.13333	16	8
5	1.25	30	0.00833	0.2	24	8
6	1.25	60	0.00833	0.4	48	8
7	1.25	20	0.00833	0.13333	16	12
8	1.25	30	0.00833	0.2	24	12
9	1.25	60	0.00833	0.4	48	12
10	1.875	20	0.0125	0.13333	10.6667	4
11	1.875	30	0.0125	0.2	16	4
12	1.875	60	0.0125	0.4	32	4
13	1.875	20	0.0125	0.13333	10.6667	8
14	1.875	30	0.0125	0.2	16	8
15	1.875	60	0.0125	0.4	32	8

Table 4.4 Cont.

16	1.875	20	0.0125	0.13333	10.6666	12
17	1.875	30	0.0125	0.2	16	12
18	1.875	60	0.0125	0.4	32	12
19	2.5	20	0.01667	0.1333	8	4
20	2.5	30	0.01667	0.2	12	4
21	2.5	60	0.01667	0.4	24	4
22	2.5	20	0.01667	0.1333	8	8
23	2.5	30	0.01667	0.2	12	8
24	2.5	60	0.01667	0.4	24	8
25	2.5	20	0.01667	0.1333	8	12
26	2.5	30	0.01667	0.2	12	12
27	2.5	60	0.01667	0.4	24	12

Serrated geometries are shown in Figure 14.
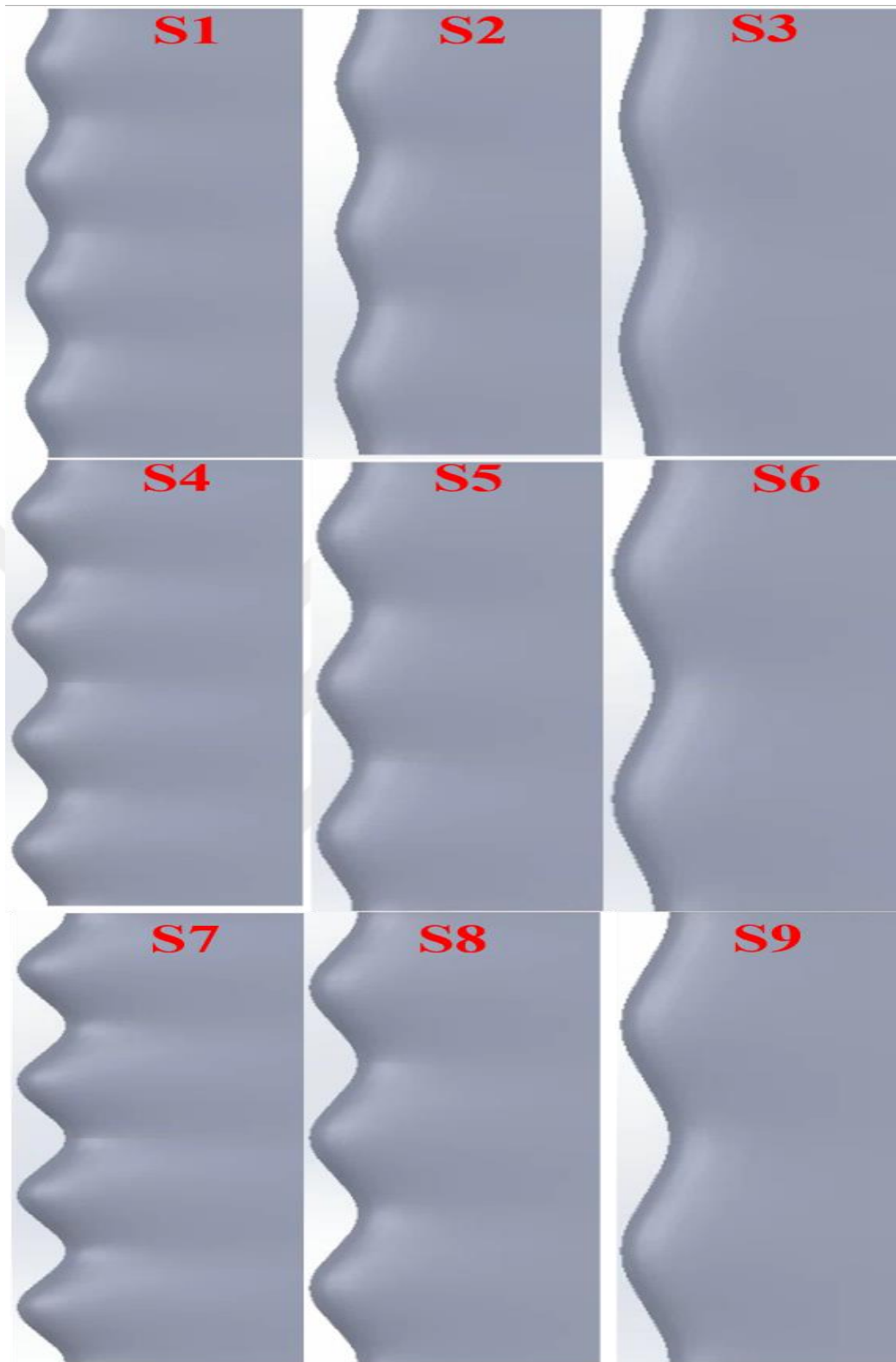
Figure 14: Naca0012 Modificated profiles

5. MANUFACTURING AND EXPERIMENTAL SETUP

Within the scope of this thesis, the effect of serrated airfoil on the flow characteristics of the wind turbine airfoil at low Reynolds number flows was investigated. The NACA0012 airfoil, which is used in wind turbines and aircraft wings, was chosen as the wing profile. Sinoidal serrations have been added on the selected airfoil. With the experimental studies, firstly, force tests were carried out and lift and drag forces were determined. In order to demonstrate the aeroacoustic behavior, sound pressure distributions were obtained by using a microphone. The experiments were carried out in the wind tunnel in the Mechanical Engineering Laboratory of TOBB University of Economics and Technology. Airfoil production was made on a 5-dimensional CNC machine using aluminum.

5.1 EXPERIMENTAL METHODS

Experiments were carried out in the wind tunnel of TOBB University of Economics and Technology Mechanical Engineering Laboratory, which has a suction type wind tunnel with speed control in the test room with the control panel. The tunnel is a closed type subsonic wind tunnel with a 300 x 300 mm test chamber. With the help of the balance system, carrying, drag and moment forces were measured by repeating the numerical studies at the same Re number and under the same conditions. Acoustic measurements were carried out by placing a microphone in the test room. In the measurements made in the test room, it was observed that the tunnel had a turbulence density of 0.74 percent at the freestream flow rate. Given in Figure 15.

Figure 15: Experimental setup in which experimental studies are carried out

5.2 MANUFACTURING FOR EXPERIMENTAL STUDY

In order to carry out the experiments, 7 different prototype blades were produced using 5-axis CNC. The blades are made of aluminum, thus reducing the surface roughness to a minimum. Airfoils of three different amplitudes and wavelengths are given in Figure 16.

Figure 16: Reference airfoils produced for experimental studies.

5.3 VELOCITY MEASUREMENT

A hot-wire anemometer with a 16-bit resolution and 50 kHz sampling frequency was used for velocity measurement. In the experimental study at TOBB University of Economics and Technology Fluid Mechanics Laboratory, the turbulence intensity in the test room of the empty tunnel was determined first. Afterwards, experimental studies were carried out. The average velocity distribution in the test region is given in Figure 17.
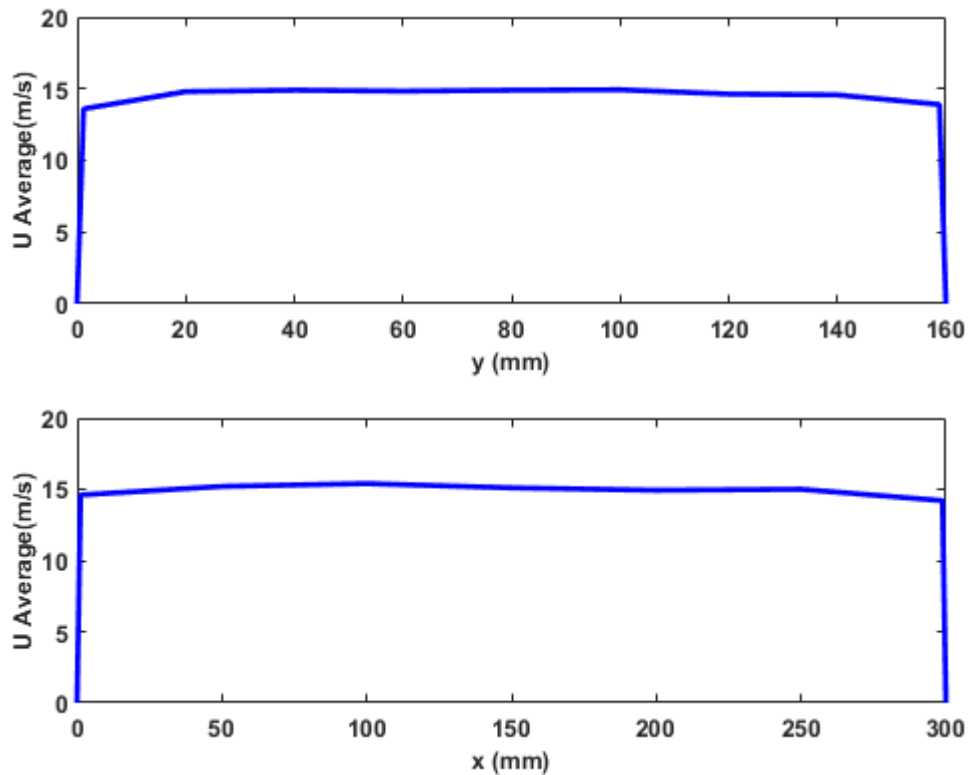
Figure 17: Time average velocity at the center of the test zone in the horizontal and vertical directions

There are many different types of hot wire anemometer (uniaxial, biaxial, boundary layer probe, etc.) specific to experiments. Experiments were made with a uniaxial probe. Figure 18 shows the hot wire anemometer probe closely.
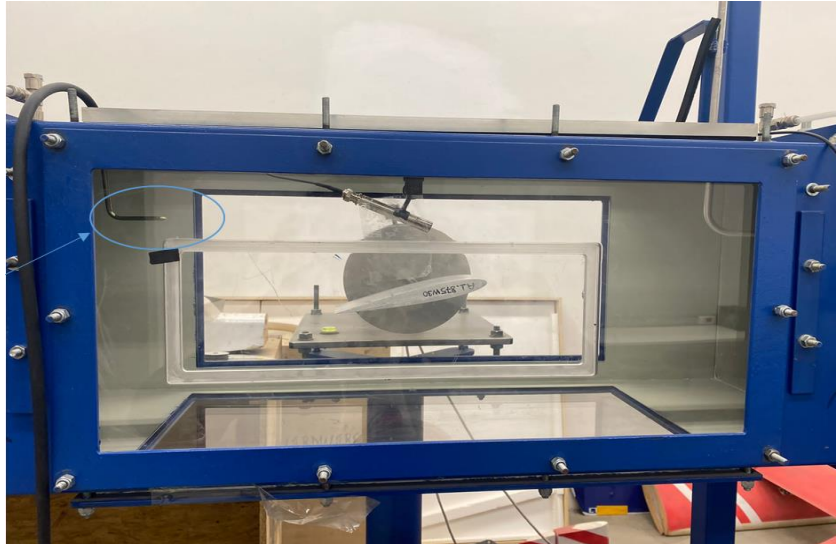
Figure 18: Hot wire anemometer.

Figure 18 also shows the airfoil with 8° angle of attack placed in the test chamber. The same image is also featured on the microphone positioned on the wing.

5.4 AERODYNAMIC FORCE MEASUREMENT FOR EXPERIMENTAL STUDIES

In determining the wing performance, the lift, drag force and pitching moment on the wing are evaluated. Dimensionless force coefficients are obtained by dividing these forces by the wing area and the dynamic pressure. The force measurement system is shown in Figure 19. The working principle of this system is based on the Wheatstone bridge.

Figure 19: Force Measurement System

5.5 AEROACOUSTIC FORCE MEASUREMENT FOR EXPERIMENTAL STUDIES

Acoustic measurements were taken using a polar microphone. Sound pressure levels are calculated in decibels as given below.

$$PSD(f) = 10log\left(S_{pp}(f)/p_{ref}^2\right) \qquad 5.1$$

Acoustic signals were measured at 20 second intervals. The microphone was placed in three different positions and was positioned on the wing, where the highest sound levels were observed, and the work continued in this way. The microphone position is visualized in Figure 20.
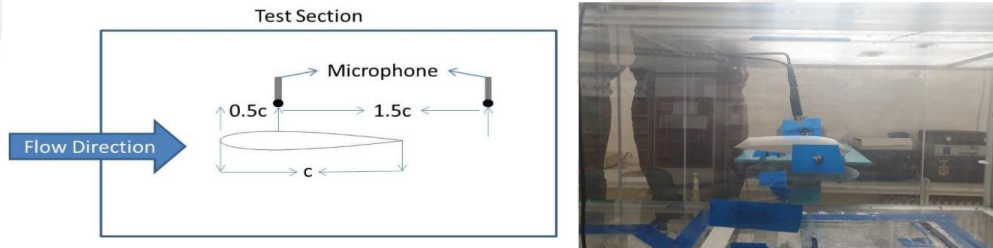
Figure 20: Receiver Locations

The experiments were investigated according to the strouhal number, which is a dimensionless parameter. Strouhal number is a dimensionless value used to analyze oscillating unsteady fluid flow dynamics problems.[52].

Strouhal number can be expressed as:

$$St = \frac{\omega l}{v} \qquad 5.2$$

The "St" given in the equation represents the Strouhal number. Other parameters w represent the oscillation frequency, l the characteristic length, and v the flow rate. The Strouhal number can be important when analyzing unsteady and oscillating flow situations in a flow problem. The Strouhal number represents a measure of the ratio of the inertial forces due to local acceleration or instability of the flow to the inertial forces due to changes in velocity from one location in the flow field to another.

6.   RESULTS

To suppress the tonal noise effectively, wave geometry, location of the serration, inflow speed, profile shape and angle of attack are the most important parameters that should be optimized. For that purpose in this part of the research the effect of the several important parameters in aerodynamic and aeroacoustics performance is given in detail according to the results obtained by the experimental and numerical studies.

6.1 AERODYNAMIC BEHAVIOR OF THE CLEAN AND SERRATED WINGS

Velocity distributions at different angles of attack are shown for the NACA0012 clean profile in Figure 21. The flow separation in the wavy leading edge airfoil occurs later than the conventional NACA0012 airfoil, especially for the high angles of attack. Increasing angle of attack to 12°, a separation zone is developed on the upper surface of the profile. Leading edge undulations deflects the oncoming air into the root region and deflection is delayed which also means that transition from a laminar to a turbulent flow is also delayed

.
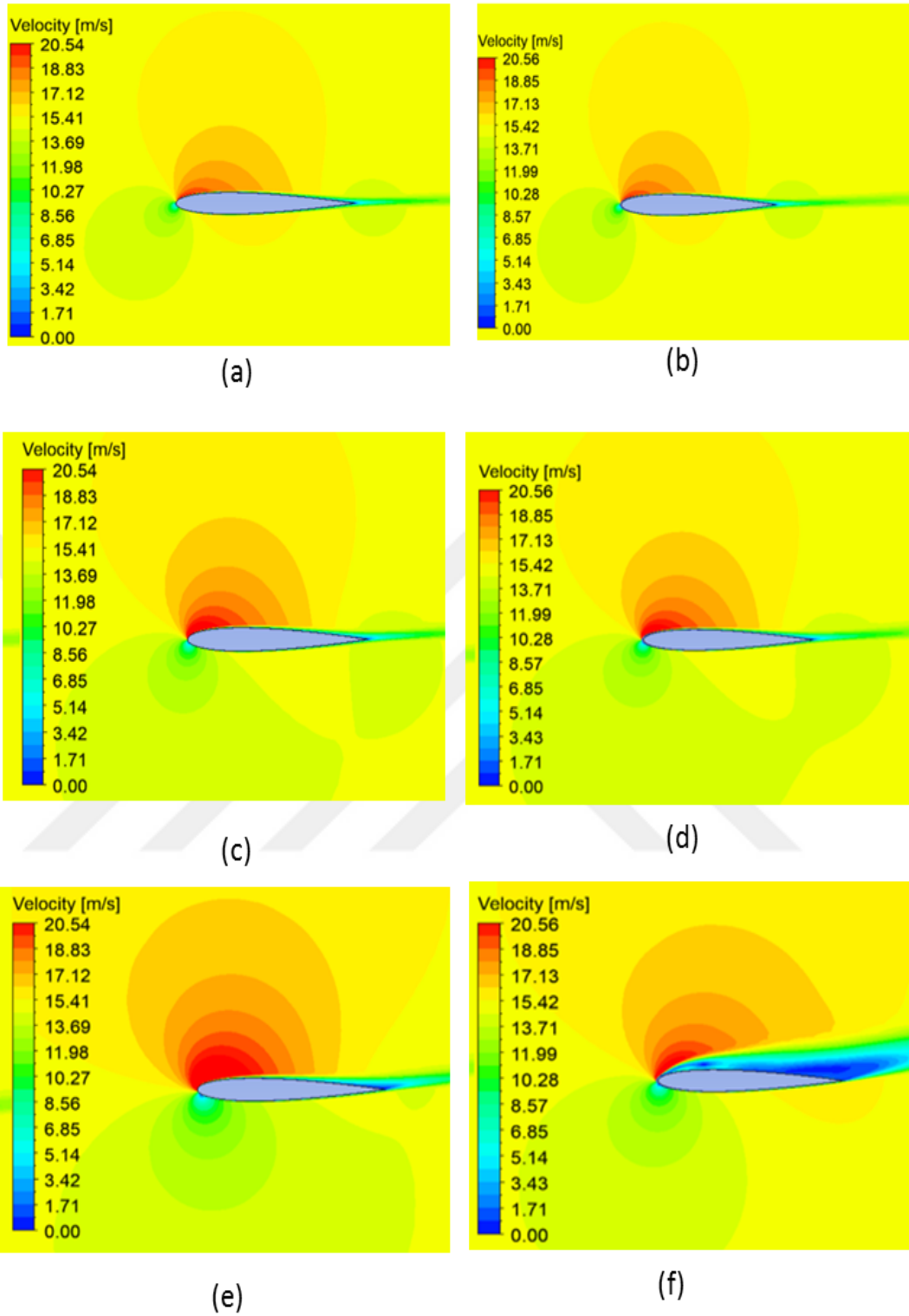
Figure 21: Contours of instantaneous velocity (a) A2.5W30 NACA Profile, aoa= 4°, (b) Base NACA Profile, aoa=4°, (c) A2.5W30 NACA Profile, aoa= 8°, (d) Base NACA Profile, aoa=8°, (e) A2.5W30 NACA Profile, aoa=12°, (f) Base NACA Profile, aoa=12°,

The separation and laminar-turbulent transition is directly related with the shear layer behavior and force characteristics of the airfoil for different angles of attack. As it is shown in Figure 22, experimental mean drag and mean lift coefficients are depicted. At smaller angle of attack values, aoa<12°, the lift and drag coefficient values are almost same for both clean and wavy profiles. On the other hand, typically for aoa>14°, also means that after stall increasing the angle of attack, the behavior is changed. For both of the profiles, after stall CL decreases and CD increases drastically. A larger value for CD and lower value for CL is obtained for wavy profile when compared with the base profile. When the velocity distribution is examined the low velocity zone region is extended in the upper side of the airfoil which results higher pressure values and smaller pressure difference between suction and pressure side. That is the situation that causes smaller lift values. The only abrupt drop of lift is observed in the stall angle, at other angles of attack values lift reduction is maximum %0.21.
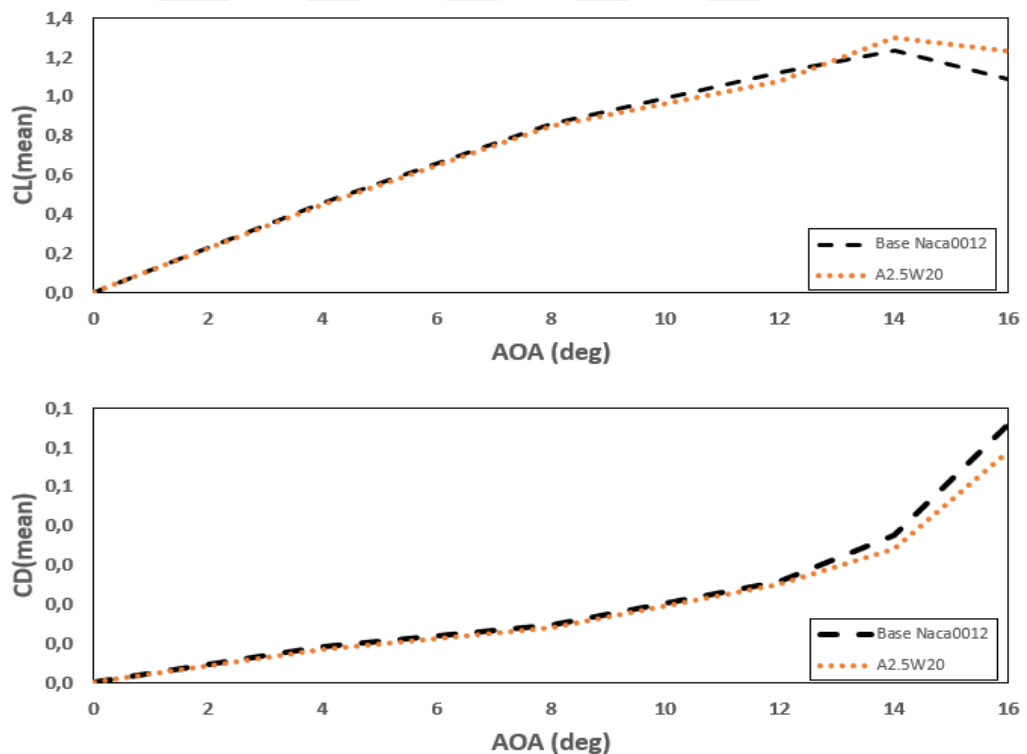
Figure 22: Force coefficient distributions for NACA0012 and A2.5W20 profile (a) Mean drag (b) mean lift coefficients

In Figure 23, instantaneous Q iso-surfaces shown for NACA0012 and A2.5W20 at aoa=12°. For both of the cases, periodic flow behavior and vortex shedding are observed. When serration is introduced shape of the shedding vortices turns to the wavy-vortices. The wavy shape vortices are break up in the trailing edge of the airfoil and roll up into new vortex structures. In the NACA0012 profile flow separation is the laminar separation while in the wavy profile it turns to turbulent separation. With wavy leading edge, as the characteristic of the separation is changed, the thickness of the boundary layer gets thinner, comprising a large momentum inside the boundary layer.
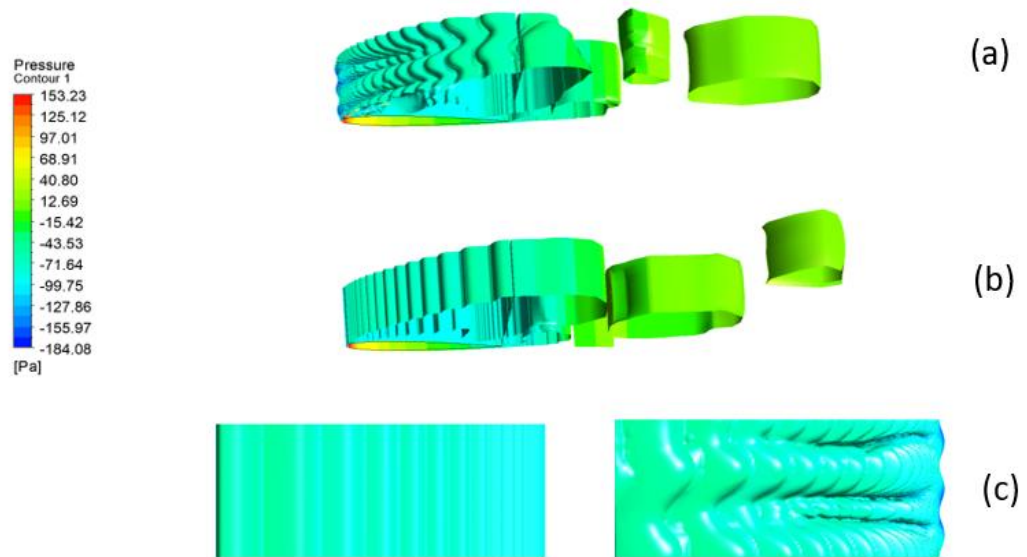
Figure 23: Instantaneous three-dimensional coherent structures for AOA=16° (a) NACA 0012 (b) Wavy airfoil

6.2 AEROACOUSTICS BEHAVIOR OF THE CLEAN AND SERRATED WINGS

Figure 24 depicts the sound pressure level distribution of the base airfoil at different speeds. Free stream velocities are varied as 5, 10, and 15 m/s. As the Reynolds number increases, the primary frequency mode value also increases. The amplitude of the primary mode known as tone intensity is increased up to %42 when velocity is rises from 5 to 10 m/s. But, when velocity reaches to 15 m/s value, the amplitude of the primary mode reduces. Therefore, it is claimed that there is no proportional relationship between the frequency amplitude and the Reynolds number. It is also seen

that, for all of the Reynolds numbers with the rise of the Strouhal number SPL values reduces as self-noise start to dominates the system.
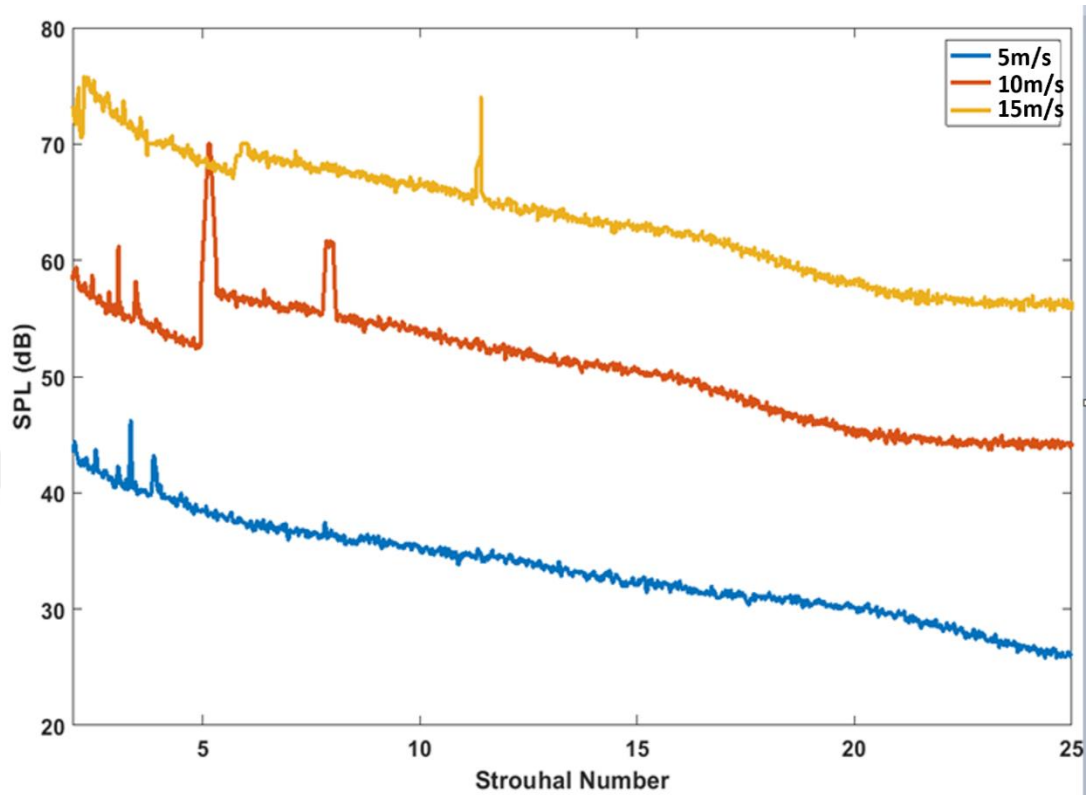

Figure 24: SPL value distribution for different free stream velocities for clean NACA profile

Figure 25 shows the frequency-dependent sound pressure level distribution for a freestream velocity of 15 m/s at different angles of attack. According to the results, no primary frequency is captured when the angle of attack is 0°. On the other hand, when angle of attack is increased to 4°, primary frequency mode is observed around St=0.68. With the increase of the angle of attack, primary mode Strouhal number also shifts toward and rises. This figure further shows that, the average sound pressure levels increase depending on the increase in the angle of attack. The harmonic instability noise trend is almost same for different angle of attack values. Also maximum noise reduction gets smaller with increasing the angle of attack. The angle of attack effect is dominant in the region where interaction noise dominates the system acoustic levels.
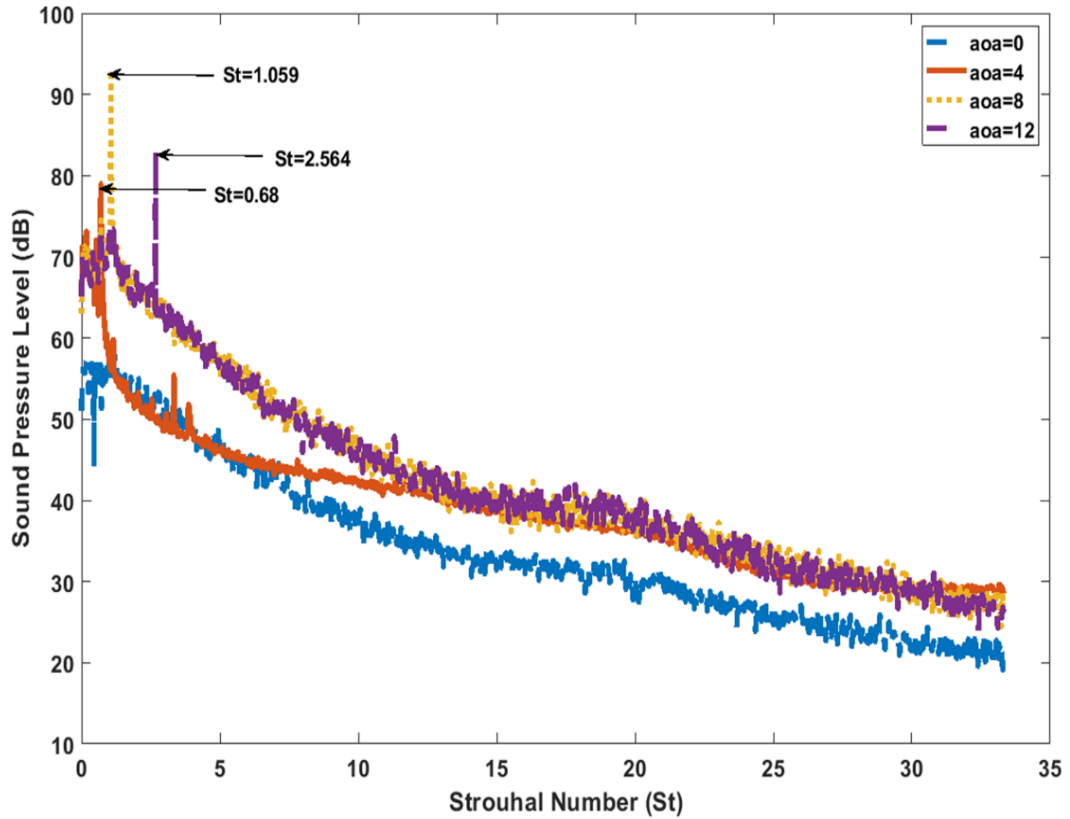
Figure 25: SPL distribution of base NACA profile for different angle of attacks

The effect of a wavy leading edge with different amplitude values is shown in Figure 26. The sound pressure level decreases consistently increase with the amplitude. A2.5W20 and A1.25W20 decrease the SPL values by about 6.5dB and 3.2dB, respectively. The reduction of SPL is more obvious in low to mid-frequency range where St<10. Better noise reduction is achieved by increasing the serration amplitude.
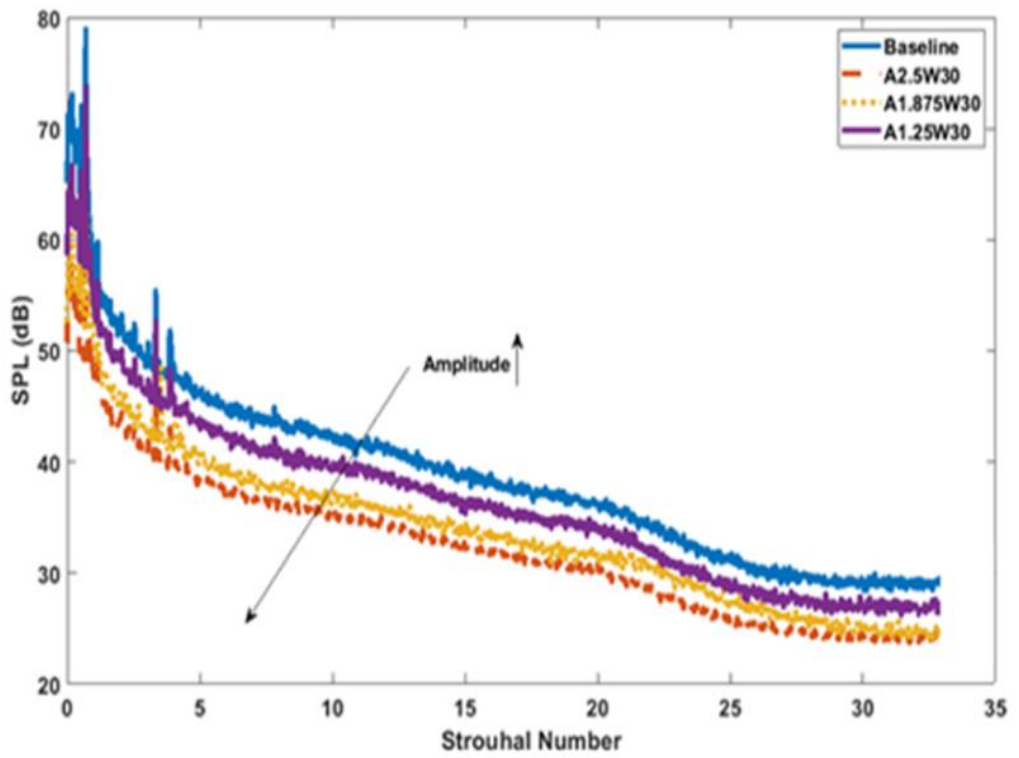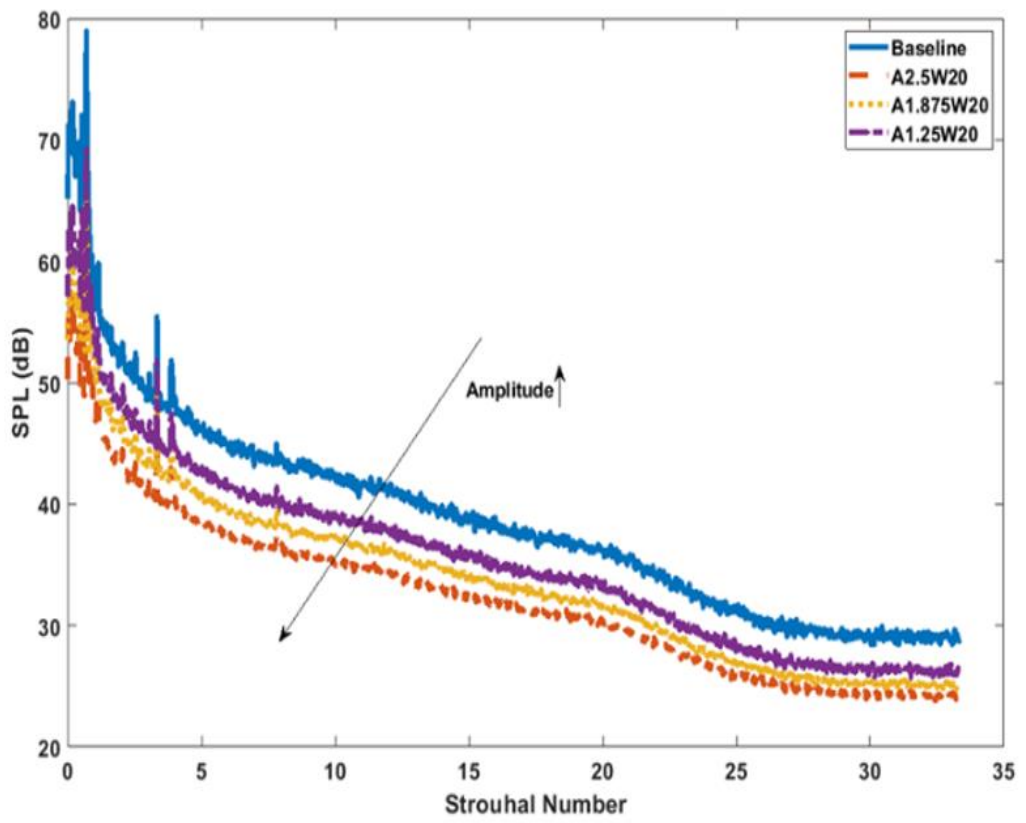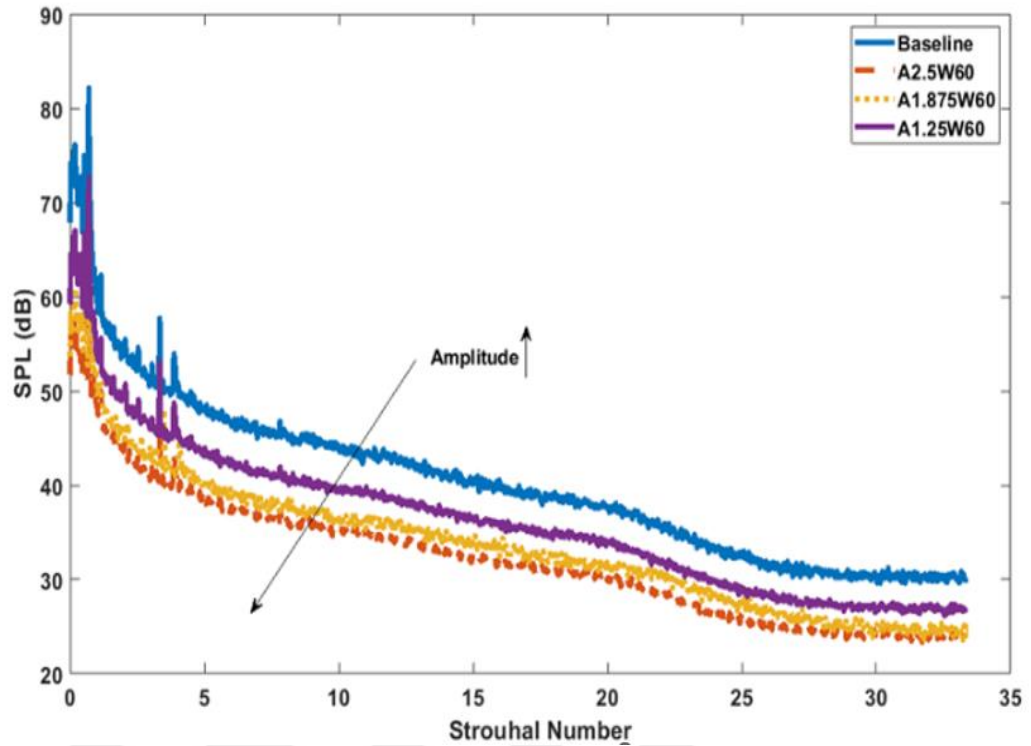
Figure 26: Comparison of acoustic performance between the base case and wavy leading-edge case

In Figure 27, TKE contour is shown for the profiles with different serration amplitudes. It is noteworthy that in the base case, in the spanwise direction there is a uniform flow topology while for the wavy cases counter-rotating vortices are generated. The volume of the vortex gets larger with increasing the amplitude. Vortices that are created because of the waviness causes momentum exchange in the boundary layer. With examining the Figure 26 and Figure 27 together, it can be said that, more turbulence fluctuations and momentum exchange in the boundary layer provide better acoustic performance. The generated vortices in higher amplitudes cause adverse pressure gradient thus improving the airfoil performance. In the smaller amplitude values post-stall performance is better than the configurations with higher amplitude.

48

Base Profile

(a)

A2.5W20

(b)

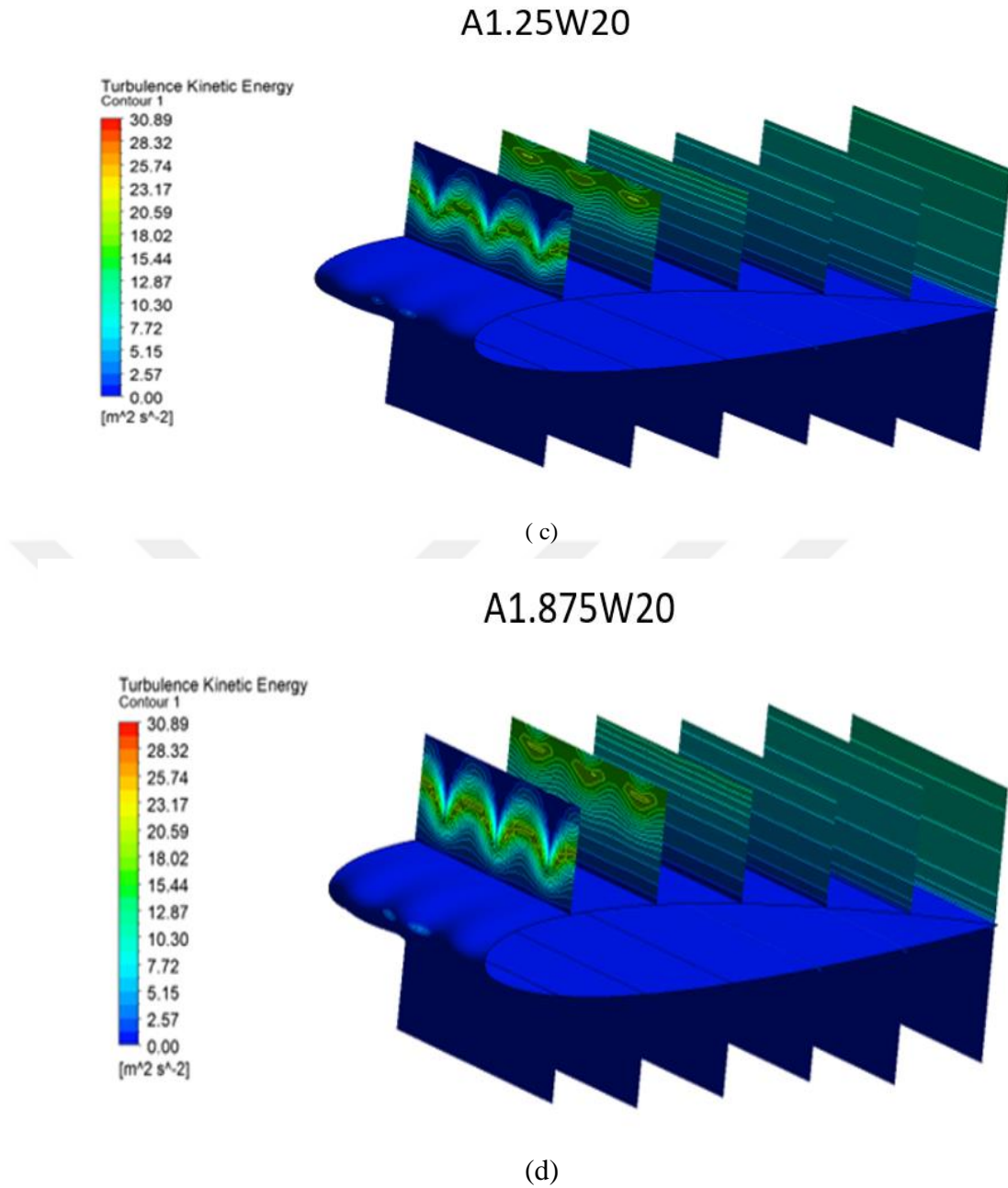## A1.25W20

(c)

A1.875W20

(d)
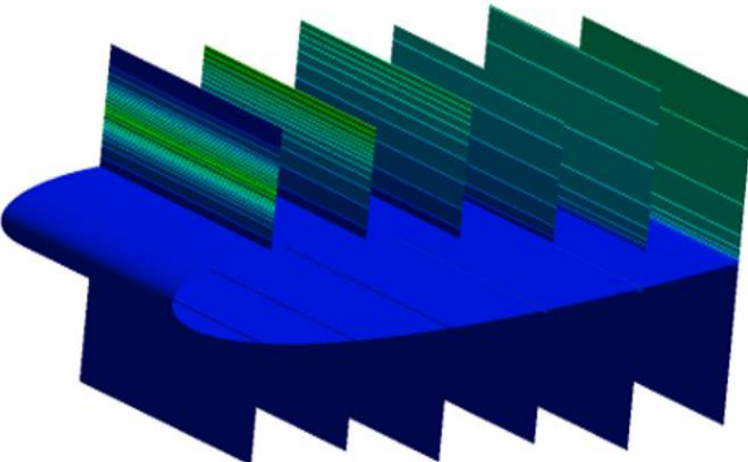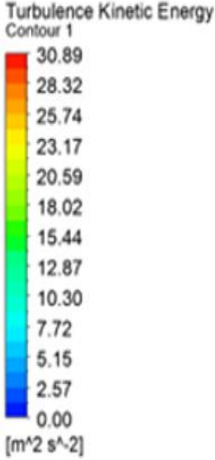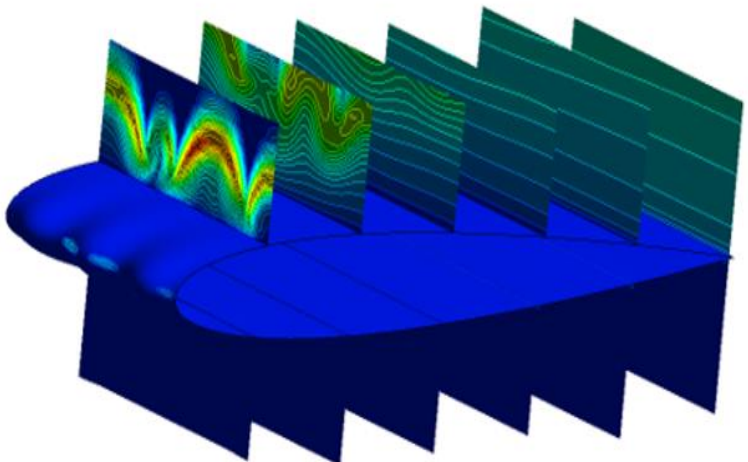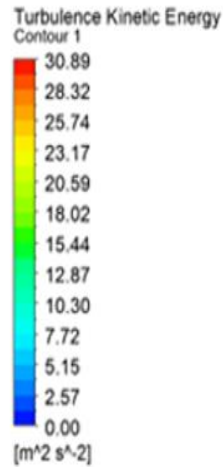
Figure 27: Turbulence kinetic energy distribution for (a) NACA0012 (b)A2.5W20 (c)A1.25W20 (d)A1.875W20 cases at an angle of attack 16°

The alteration of the acoustic performance is visible when the wavelength of the serration is varied as shown in Figure 28. It is clear that, tonal noise with a larger amplitude and smaller wavelength has a major SPL reduction effect when compared to the other serration configurations. With increasing the amplitude value, the effect of the wavelength on tonal noise suppression is decreased.
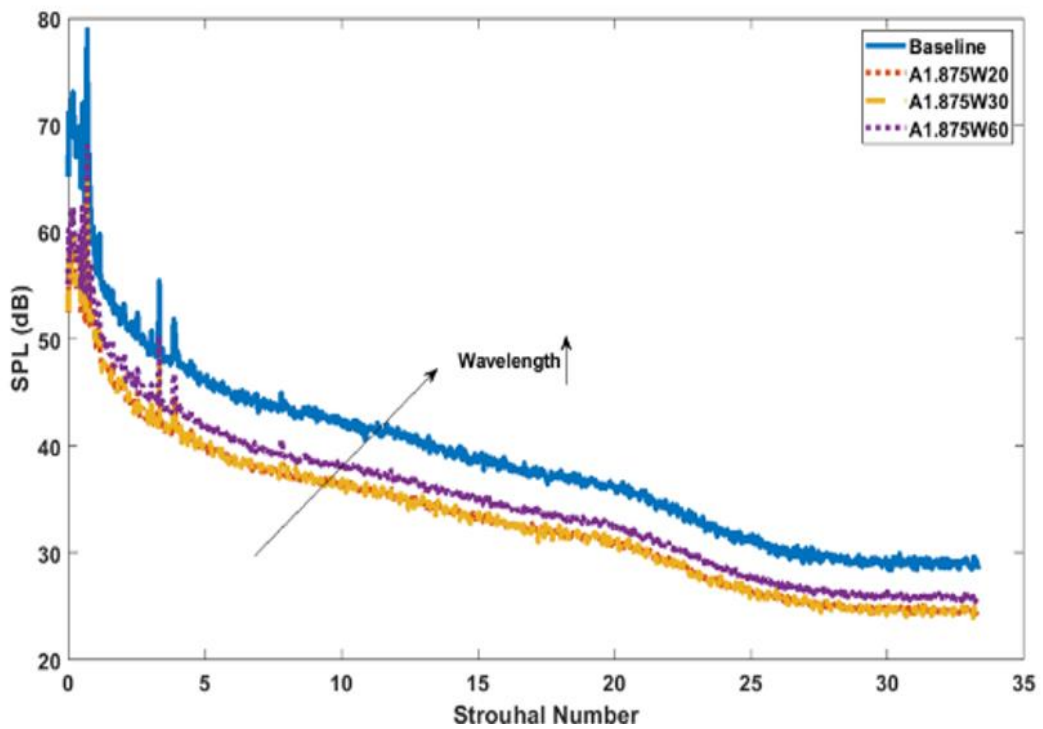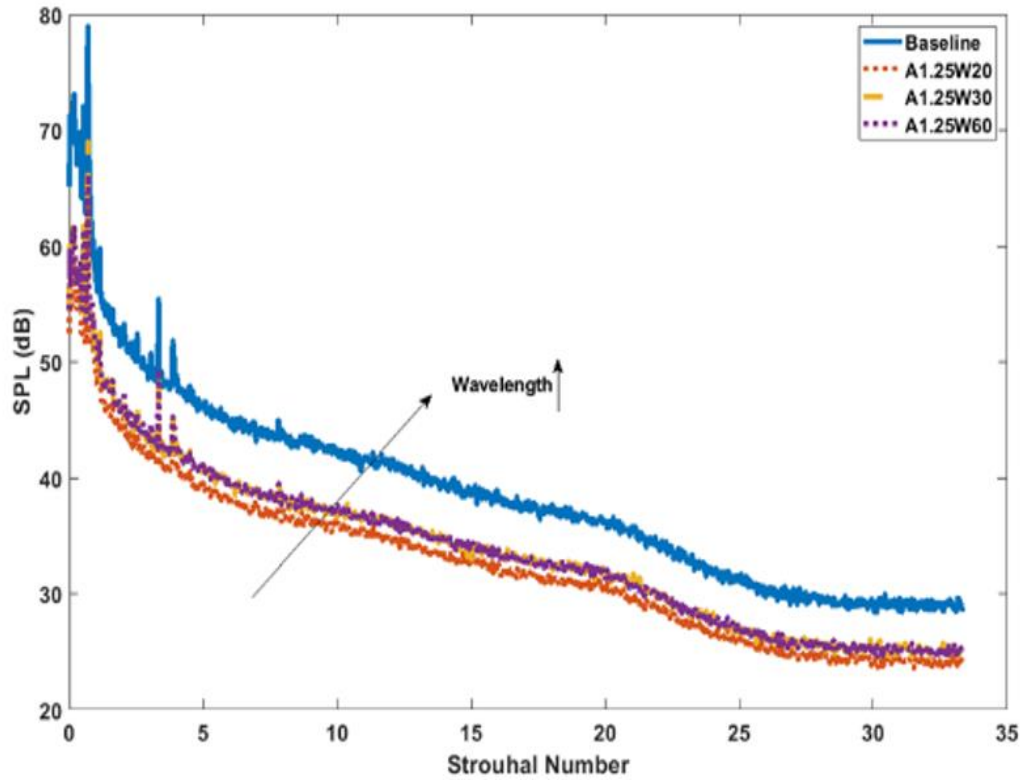
Figure 28: Comparison of acoustic performance between base case and wavy leading-edge case with different wavelength

With creating serrations the incoming flow deflected through the thoughts of the serrations and produces vortex structures. As it is seen in Figure 29, with smaller wavelengths the number of vortices increases and flow is broken down to more

energizing zones between the peaks (in the tip region) of the serrations. Those more energetic particles that induce momentum into flow, keeps the flow reattaching over the peak region with delaying the flow separation. As it is illustrated in Figure 29, when wavelength is decreased to 20 mm, 4 vortex zones are originated in the pit regions that reduces the SPL levels up to %24.04 due to the more momentum transfer. Also claimed in the research of Miklosovich et al [8] and Lohry et al [29], serrations working mechanism is similar to the vortex generators.
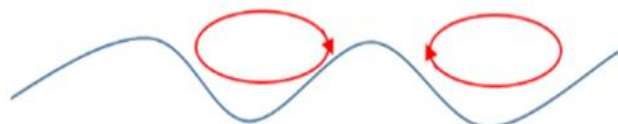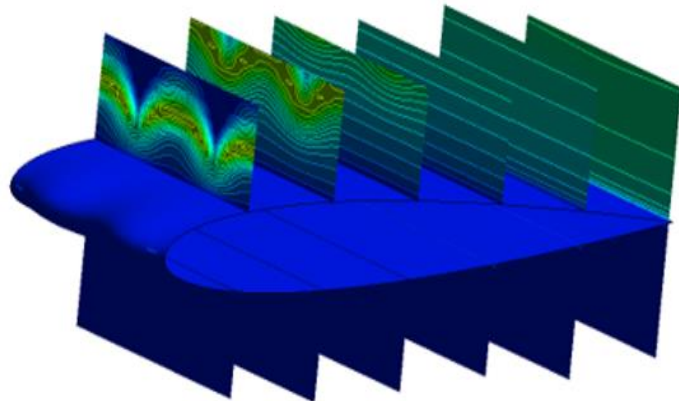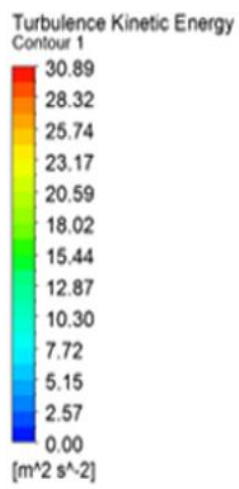
Base Profile
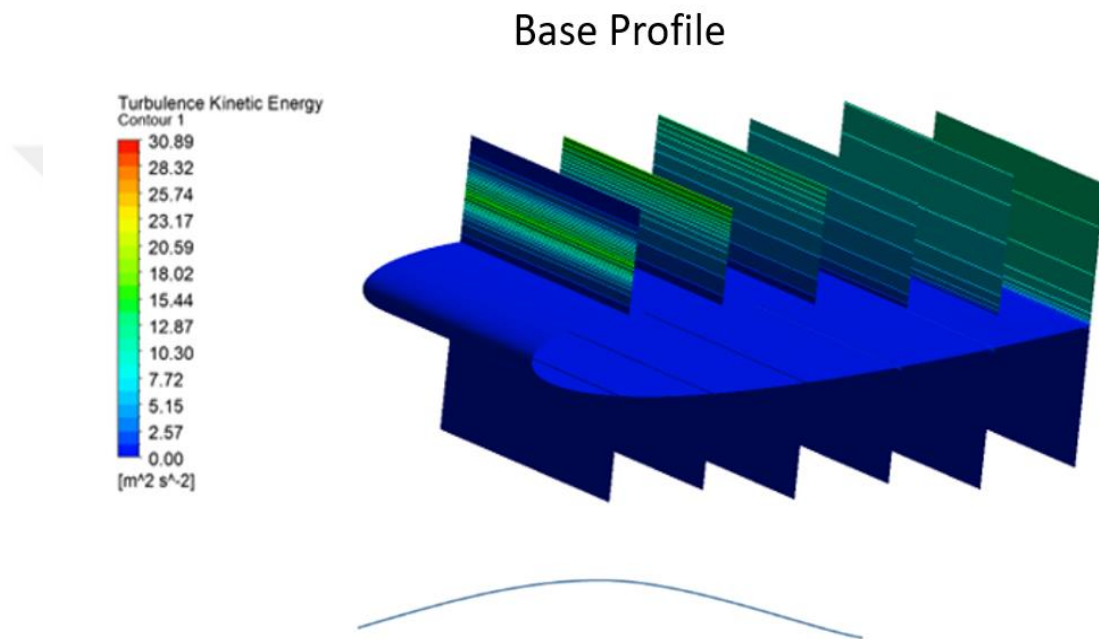
(a)

A2.5W60

(b)

A2.5W30

(c)

A2.5W20

(d)
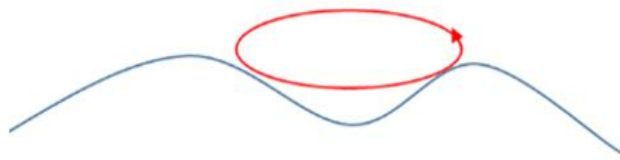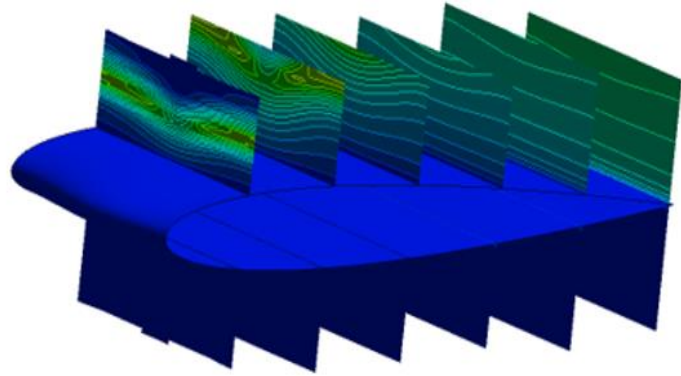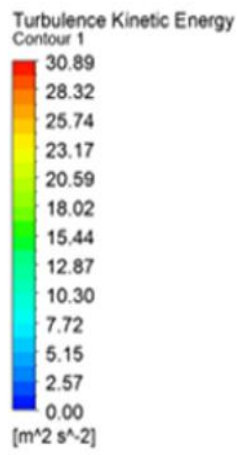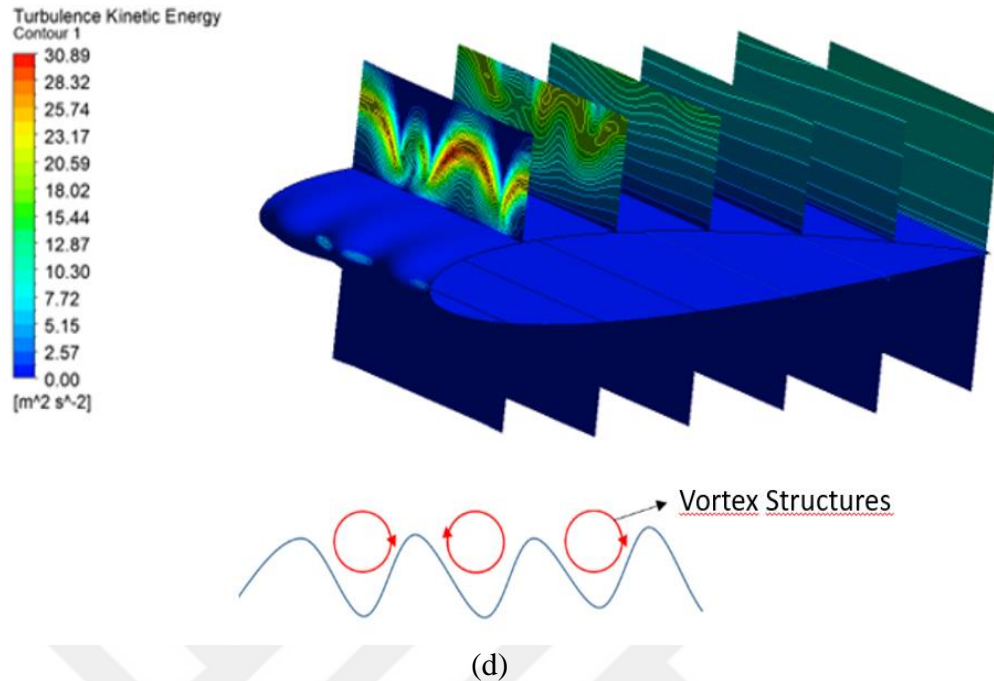
Figure 29: Turbulence kinetic energy distribution for 8(a) NACA0012 (b) A2.5W60 (c)A2.5W30 (d)A2.5W20 cases at an angle of attack 16°

In Figure 30 and Table 6.1, SPL reduction level for all the configurations is given for both experimental and numerical study. It is seen that, numerical results are matched with experiments with maximum 4% error. It is obvious that, leading-edge serration provides substantial noise reduction levels. For the cases with small wavelength and larger amplitudes, the effectiveness of the serration rises up to 24% noise reduction levels. It is seen that in smaller amplitude values, the effect of the wavelength is negligible. The noise suppression effect of wavelength becomes dominant at higher amplitude values. In conclusion, it is seen that maximum noise reduction is function of amplitude and wavelength. It should also be noted that wavelength is also function of the amplitude.
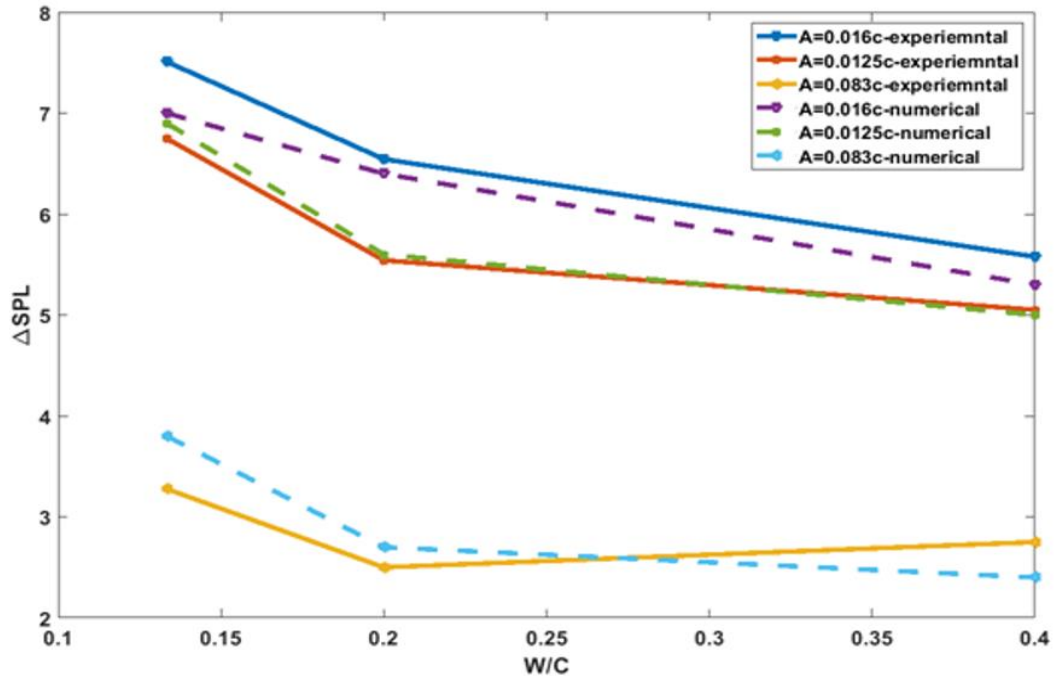
Figure 30: Variation of sound pressure level for different configurations

Table 6.1: SPL reduction in percentage for the experimental and numerical study

Modified Cases	%Reduction Experimental Result	%Reduction Numerical Result
A2.5W20	24.04	23.87
A2.5W30	20.32	19.9
A2.5W60	16.81	15.05
A1.875W20	21.09	22.14
A1.875W30	16.69	16.95
A1.875W60	14.99	16.54
A1.25W20	9.24	10.25
A1.25W30	6.90	7.25
A1.25W60	7.64	6.54

7. CONCLUSION

In this study, to determine the optimum serration geometry configuration, extensive experimental and numerical studies are carried out for NACA0012 airfoil profile. The main finding of the research can be given as follows:

- For the base profile, increasing the Reynolds number, increases both the average SPL distribution and amplitude of the primary modes.

- It is shown that, with increasing the angle of attack, noise levels get higher. The best noise reduction is achieved when aoa=0°, as there is no primary mode observed in the flow.

- Implementing serration with a larger amplitude and smaller wavelength has the best aeroacoustic characteristics. With the smaller wavelengths more vortices are generated in the tip regions. And with the higher amplitudes the flow concentration in the tips is increased. Insight of this, it can be said that, breaking the flow to the smaller vortices with higher concentrations increases the velocity and higher suction pressure in the flow region. That's the reason why smaller wavelength and larger amplitude airfoil configurations give better aeroacoustic performance.

- The finding revealed that, although serrations have a great effect on suppression of tonal noise, it has adverse effects on the aerodynamic performance especially in the pre-stall region. However, in the post-stall regime, serrations produce a high lift coefficient by as much as %17.

- The underlying flow physics of serration is similar to the vortex generators, but a deeper understanding is required. With adding serration, the flow flows through the leading edge deflected to the tips and vortices are generated in that region. With the interaction of the vortices with the free streamflow, flow is energized, and momentum transfer has occurred.

- Numerical predictions that are carried out using the LES are agreement with the experimental results. However, to capture the flow behaviour, better DNS is needed to be used for this problem.

- The wavelength effect on noise suppression is function of the amplitude. In the higher amplitude values, increasing the wavelength has a negligible effect on the aeroacoustic performance.

  Significant noise reduction is observed in the region between 3<St<20.

The key challenge in the optimization of the serration geometry is also finding a configuration that does not reduce the aerodynamic performance of the system. Therefore, a systematic parametric study is needed to find the optimum case.

REFERENCES

[1] Michael James Lighthill (1952). "On Sound Generated Aerodynamically I: General Theory", *Proceedings Of The Royal Society*, 564-587.

[2] Michael James Lighthill (1952). "On Sound Generated Aerodynamically I: General Theory", *Proceedings Of The Royal Society*, 564-587.

[3] Vincenc Strouhal (1878). "Ueber Eine Besondere Art Der Tonerregung" (On An Unusual Sort Of Sound Excitation). *Annalen Der Physik Und Chemie*, *3rd Series, 5 (10),* 216–251.

[4] Michael James Lighthill (1954). "On Sound Generated Aerodynamically. II. Turbulence As A Source Of Sound", *Proceedings Of The Royal Society Of London. Series A, Mathematical And Physical Sciences* Pp. 1-32.

[5] Ian Proudman (1952). "Sound Generation Of Noise By İsotropic Turbulence", *Proceedings Of The Royal Society,* 119-132.

[6] Newby Curle. (1955). "The İnfluence Of Solid Boundaries Upon Aerodynamic Sound", *Proceedings Of The Royal Society A,* 505-514.

[7] Williams JE Ffwocs & David Hawkings (1969). "Sound Generation By Turbulence And Surfaces İn Arbitrary Motion", *Philosophical Transactions Of The Royal Society Of London, Series A, Vol. 264, No. 1151,* 321-342.

[8] Thomas Brooks, Dennis Pope, & Michael Marcolini. (1989). *NASA Reference Publication 1218: Airfoil Self-Noise And Prediction.* NASA.

[9] Thomas Brooks, Dennis Pope, & Michael Marcolini. (1989). *NASA Reference Publication 1218: Airfoil Self-Noise And Prediction.* NASA.

[10] Thomas Brooks, Dennis Pope, & Michael Marcolini. (1989). *NASA Reference Publication 1218: Airfoil Self-Noise And Prediction.* NASA.

[11] Wagner Claus & Thomas Hüttl (2002). "LES For Acoustics", *Proceedings Of The International Workshop* On "LES For Acoustics, 7–8 October, German Aerospace Center, DLR, Göttingen, Germany, DGLR Report 2002-03.

[12] Michael James Lighthill (1952). "On Sound Generated Aerodynamically I: General Theory". *Proceedings Of The Royal Society*, 564-587.

[13] Michael James Lighthill (1954). "On Sound Generated Aerodynamically. II. Turbulence As A Source Of Sound", *Proceedings Of The Royal Society*

[14] Newby Curle. (1955). "The İnfluence Of Solid Boundaries Upon Aerodynamic Sound", *Proceedings Of The Royal Society A,* 505-514.

[15] Alan Hersh & Richard Hayden (1971). "Aerodynamic Sound Radiaton From Lifting Surfaces With And Withoud Leading-Edge Serrations", *BBN Rep. No. 2095*

[16] Roger Arndt & Robert Nagel (1972). "Effect Of Leading Edge Serrations On Noise Radiaton From A Model Rotor", *AIAA Paper No. 72-655*.

[17] Alan Hersh & Richard Hayden (1971). "Aerodynamic Sound Radiaton From Lifting Surfaces With And Withoud Leading-Edge Serrations", *BBN Rep. No. 2095*

[18] Roger Arndt & Robert Nagel (1972). "Effect Of Leading Edge Serrations On Noise Radiaton From A Model Rotor", *AIAA Paper No. 72-655*.

[19] Michael Howe (1991). "Aerodynamic Noise Of A Serrated Trailing Edge", *Journal Of Fluids And Structures, Vol.5(1),* 33-45.

[20] Michael Howe (1991). "Noise Produced By A Sawtooth Trailing Edge", *Journal Of The Acoustical Society Of America, Vol.90*, 482-487.

[21] Lloyd Jones & Richard Sandberg (2009). "Direct Numerical Simulations Of Noise Generated By The Flow Over An Airfoil With Trailing Edge Serrations", *15th AIAA/CEAS Aeroacoustics Conference (30th AIAA Aeroacoustics Conference),* Miami, Florida, USA : May 11-13.

[22] Chong Tze Pei & Phillip Joseph (2010). "An Experimental Study Of Airfoil İnstability Noise With Trailing Edge Serrations", *15th AIAA/CEAS Aeroacoustics Conference (30th AIAA Aeroacoustics Conference),* Stockholm, Sweden : June 7-9.

[23] Chong Tze Pei & Philliph Joseph (2013). "Airfoil Self Noise Reduction By Non-Flat Plate Type Trailing Edge Serrations", *Applied Acoustics, Vol. 74,* 607-613.

[24] Kristy Hansen, Richard Kelso & Con Doolan 2010. "Reduction Of Flow-İnduced Tonal Noise Through Leading Edge Tubercle Modifications." In: 16th AIAA/CEAS Aeroacoustic Conference, Stockholm, Sweden. Reston: AIAA, P. 1–10.

[25] Clair, Vincent, Et Al. 2013 "Experimental And Numerical İnvestigation Of Turbulence-Airfoil Noise Reduction Using Wavy Edges". *American Institute Of Aeronautics And Astronautics Journa*l, 55(11), 2695-2713.

[26] Paruchuri, Chaitanya, Et Al. 2015. "Broadband Noise Reduction Through Leading Edge Serrations On Realistic Aerofoils", AIAA Aviation, 2Dallas, 21st AIAA Aeroacoustic Conference.

[27] Miklosovic David, Mark Murray, Howle Laurens, Fish Frank. 2004 "Leading-Edge Tubercles Delay Stall On Humpback Whale (Megaptera Novaeangliae) Flippers." Physics Of Fluids, 16(5).

[28] Miklosovic David, Mark Murray, Howle Laurens, 2007 "Experimental Evaluation Of Sinusoidal Leading Edges." *Journal Of Aircraft*, 44(4):1404-1408.

[29] Stanway Michael Jordan , 2008. "Hydrodynamic Effects Of Leading-Edge Tubercles On Control Surfaces And İn Flapping Foil Propulsion" .Phd Thesis, Massachusetts Inst. Of Technology, Cambridge, MA.

[30] Skillen Alex, Et Al. 2014. " Flow Over A Wing With Leading-Edge Undulations". *AIAA Journal*, 53(2),1–9.

[31] Pinelli, Alfredo Et Al. 2012. "Control Of The Separated Flow Around An Airfoil Using A Wavy Leading Edge İnspired By Humpback Whale Flippers". Comptes Rendus Mcanique, 340(1-2):107114.

[32] Narayanan, Subramanian Et Al. 2015. "Airfoil Noise Reductions Through Leading Edge Serrations", Physics Of Fluids, 27 (2), 025109-[17pp].

[33] Rao, Chen Et Al. 2017. "Owl-İnspired Leading-Edge Serrations Play A Crucial Role İn Aerodynamic Force Production And Sound Suppression", Bioinspir Biomim. Jul 4;12(4):046008. Doi: 10.1088/1748-3190/Aa7013.

[34] Huang, G.Y., Shiah, Y.C:, Bai, C.J:, Chong, W.T., "Experimental Study Of The Protuberance Effect On The Blade Performance Of A Small Horizontal Axis Wind Turbine", *Journal Of Wind Energy*, Vol (147), 2015, Pp:202-211

[35] Lam, K., Lin, Y. F., Liu, Y., & Zou, L. (2012). "Numerical Investigation Of Flow Past A Wavy Airfoil. In Applied Mechanics And Materials", (Vol. 110, Pp. 4269-4275). *Trans Tech Publications Ltd.*

[36] Wang Zhenyu, Mei Zhuang, "Leading-Edge Serrations For Performance İmprovement On A Vertical-Axis Wind Turbine At Low Tip-Speed-Ratios", *Applied Energy*, Vol (208), Pp: 1184-1197, 2017.

[37] Javaid, Muhammad Yasar, Et Al. Underwater Gliders: A Review, MATEC Web Of Conferences, 13, 2014.

[38] Soderman Paul T. "Leading-Edge Serrations Which Reduce The Noise Of Low-Speed Rotors", *NASA Techinical Note*, Report No. NASA TN D-7371; NASA: Washington, DC, USA, 1973.

[39] Danielle Moreau, Con Doolan, "Noise-Reduction Mechanism Of A Flat-Plate Serrated Trailing Edge", *AIAA Journal*, 51 (10),2013, Pp: 2513-2522

[40] Michael James Lighthill (1952). "On Sound Generated Aerodynamically I: General Theory", *Proceedings Of The Royal Society*, 564-587.

[41] Benini Ernesto, & Toffolo Andrea. (2002). "Optimal Design Of Horizontal-Axis Wind Turbines Using Blade-Element Theory And Evolutionary Computation", *J. Sol. Energy Eng.*, 124(4), 357-363.

[42] Benini Ernesto, & Toffolo Andrea. (2002). "Optimal Design Of Horizontal-Axis Wind Turbines Using Blade-Element Theory And Evolutionary Computation", *J. Sol. Energy Eng.*, 124(4), 357-363.

[43] Newby Curle. (1955). "The İnfluence Of Solid Boundaries Upon Aerodynamic Sound", *Proceedings Of The Royal Society A,* 505-514.

[44] Newby Curle. (1955). "The İnfluence Of Solid Boundaries Upon Aerodynamic Sound", *Proceedings Of The Royal Society A,* 505-514.

[45] Newby Curle. (1955). "The İnfluence Of Solid Boundaries Upon Aerodynamic Sound", *Proceedings Of The Royal Society A,* 505-514.

[46] Michael James Lighthill (1952). "On Sound Generated Aerodynamically I: General Theory", *Proceedings Of The Royal Society*, 564-587.

[47] Michael James Lighthill (1952). "On Sound Generated Aerodynamically I: General Theory", *Proceedings Of The Royal Society*, 564-587.

[48] Mendez Simon, (2013). "On The Use Of The Ffowcs Williams-Hawkings Equation To Predict Far-Field Jet Noise From Large-Eddy Simulations", *International Journal Of Aeroacoustics*, 12(1-2), 1-20.

[49] Piomelli Ugo. (2008). "Wall-Layer Models For Large-Eddy Simulations", *Progress İn Aerospace Sciences*, 44(6), 437-446.

[50] Piomelli Ugo. (2008). "Wall-Layer Models For Large-Eddy Simulations", *Progress İn Aerospace Sciences*, 44(6), 437-446.

[51] Piomelli Ugo. (2008). "Wall-Layer Models For Large-Eddy Simulations", *Progress İn Aerospace Sciences*, 44(6), 437-446.

[52] Ahlborn Boye, Seto Mae, Noack Bernd (2002). "On Drag, Strouhal Number And Vortex-Street Structure", *Fluid Dynamics Research*, 30(6), 379.